RESEARCH

udot.utah.gov
Utah Department of Transportation - Research Division
4501 South 2700 West - P.O. Box 148410 - SLC,UT 84114-8410

Report No. UT-16.12

LABORATORY RESILIENT MODULUS MEASUREMENTS OF AGGREGATE BASE MATERIALS IN UTAH

Prepared For:

Utah Department of Transportation
Research Division

Submitted By:

Brigham Young University
Department of Civil and Environmental Engineering

Authored By:

W. Spencer Guthrie, Ph.D.
Kirk D. Jackson

Final Report
December 2015

DISCLAIMER

The authors alone are responsible for the preparation and accuracy of the information, data, analysis, discussions, recommendations, and conclusions presented herein. The contents do not necessarily reflect the views, opinions, endorsements, or policies of the Utah Department of Transportation or the U.S. Department of Transportation. The Utah Department of Transportation makes no representation or warranty of any kind, and assumes no liability therefore. The authors also make no warranty, express or implied, regarding the suitability of findings documented in this report for a particular purpose and shall not be held liable under any circumstances for any direct, consequential, or other damages with respect to claims by users of any findings documented in this report, including claims based on allegations of errors, omissions, or negligence.

ACKNOWLEDGMENTS

The authors acknowledge the Utah Department of Transportation for funding this research. Appreciation is also given to all those who assisted with the laboratory work for this project, including Jake Tolbert, Sharlan Montgomery, Tenli Waters, Jaren Knighton, Sariann Lemon, David Anderson, and Rodney Mayo.

TECHNICAL REPORT ABSTRACT

1. Report No. UT-1X.XX	2. Government Accession No. NA	3. Recipient's Catalog No. NA
4. Title and Subtitle LABORATORY RESILIENT MODULUS MEASUREMENTS OF AGGREGATE BASE MATERIALS IN UTAH		5. Report Date December 2015 6. Performing Organization Code
7. Author(s) W. Spencer Guthrie and Kirk D. Jackson		8. Performing Organization Report No.
9. Performing Organization Name and Address Brigham Young University Department of Civil and Environmental Engineering 368 Clyde Building Provo, UT 84602		10. Work Unit No. 5H07690H 11. Contract or Grant No. 12-9110
12. Sponsoring Agency Name and Address Utah Department of Transportation 4501 South 2700 West P.O. Box 148410 Salt Lake City, UT 84114-8410		13. Type of Report & Period Covered Final Report July 2012 to December 2015 14. Sponsoring Agency Code UT 09.301

15. Supplementary Notes

Prepared in cooperation with the Utah Department of Transportation and the U.S. Department of Transportation, Federal Highway Administration

16. Abstract

The objectives of this research were to 1) determine the resilient modulus of several representative aggregate base materials in Utah and 2) investigate correlations between laboratory measurements of resilient modulus, California bearing ratio (CBR), and other properties of the tested materials. Two aggregate base materials were obtained from each of the four Utah Department of Transportation (UDOT) regions. Important material properties, including particle-size distribution, soil classification, and the moisture-density relationship, were investigated for each of the sampled aggregate base materials. The CBR and resilient modulus of each aggregate base material were also determined. After all of the data were collected, a set of independent predictor variables was analyzed using both stepwise regression and best subset analysis to develop a model for predicting resilient modulus.

For the aggregate base materials tested in this research, the average resilient modulus varied from 16.0 to 25.6 ksi. The test results show that resilient modulus and CBR are not correlated for the materials tested in this research. Therefore, a new model was developed to predict the resilient modulus based on the percent passing the No. 200 sieve, particle diameter corresponding to 30 percent finer, optimum moisture content, maximum dry density (MDD), and ratio of dry density to MDD. Although the equation may not be applicable for values outside the ranges of the predictor variables used to develop it, it is expected to provide UDOT with reasonable estimates of resilient modulus values for aggregate base materials similar to those tested in this research.

17. Key Words Aggregate Base Material, California Bearing Ratio, Mechanistic-Empirical Pavement Design, Resilient Modulus		18. Distribution Statement Not restricted. Available through: UDOT Research Division 4501 South 2700 West P.O. Box 148410 Salt Lake City, UT 84114-8410 www.udot.utah.gov/go/research		23. Registrant's Seal
19. Security Classification (of this report) Unclassified	20. Security Classification (of this page) Unclassified	21. No. of Pages 130	22. Price	

TABLE OF CONTENTS

LIST OF TABLES

LIST OF FIGURES

LIST OF ACRONYMS

AASHTO	American Association of State Highway and Transportation Officials
ASTM	American Society for Testing and Materials
CBR	California bearing ratio
CV	coefficient of variation
DOT	department of transportation
MDD	maximum dry density
MEPDG	Mechanistic-Empirical Pavement Design Guide
NCHRP	National Cooperative Highway Research Program
OMC	optimum moisture content
PI	plasticity index
RMSE	root mean squared error
UDOT	Utah Department of Transportation
USCS	Unified Soil Classification System
UTM	Universal Testing Machine

EXECUTIVE SUMMARY

The Utah Department of Transportation (UDOT) has fully implemented the *Mechanistic-Empirical Pavement Design Guide* for pavement design but has been using primarily level-three design inputs obtained from correlations to aggregate base materials developed at the national level. UDOT was interested in investigating correlations between laboratory measurements of resilient modulus, California bearing ratio (CBR), and other material properties specific to base materials commonly used in Utah; therefore, a statewide testing program was needed. The objectives of this research were to 1) determine the resilient modulus of several representative aggregate base materials in Utah and 2) investigate correlations between laboratory measurements of resilient modulus, CBR, and other properties of the tested materials.

Two aggregate base materials were obtained from each of the four UDOT regions. Important material properties, including particle-size distribution, soil classification, and the moisture-density relationship, were investigated for each of the sampled aggregate base materials. The CBR and resilient modulus of each aggregate base material were determined in general accordance with American Society for Testing and Materials D1883 and American Association of State Highway and Transportation Officials T 307, respectively. After all of the data were collected, several existing models were evaluated to determine if one or more of them could be used to predict the resilient modulus values measured in this research. Statistical analyses were also performed to investigate correlations between measurements of resilient modulus, CBR, and other properties of the tested aggregate base materials, mainly including aspects of the particle-size distributions and moisture-density relationships. A set of independent predictor variables was analyzed using both stepwise regression and best subset analysis to develop a model for predicting resilient modulus. After a suitable model was developed, it was analyzed to determine the sensitivity of the model coefficients to the individual data points.

For the aggregate base materials tested in this research, the average resilient modulus varied from 16.0 to 25.6 ksi. Regarding the correlation between resilient modulus and CBR, the test results show that resilient modulus and CBR are not correlated for the materials tested in this research. Therefore, a new model was developed to predict the resilient modulus based on the percent passing the No. 200 sieve, particle diameter corresponding to 30 percent finer, optimum

moisture content, maximum dry density (MDD), and ratio of dry density to MDD. Although the equation may not be applicable for values outside the ranges of the predictor variables used to develop it, it is expected to provide UDOT with reasonable estimates of resilient modulus values for aggregate base materials similar to those tested in this research.

1.0 INTRODUCTION

1.1 Problem Statement

Recent advances in the field of pavement design have led to the development of the *Mechanistic-Empirical Pavement Design Guide* (MEPDG) (*1*). In this design method, one of the most important inputs for the design of a pavement structure is the resilient modulus of each of the pavement layers. The MEPDG classifies the resilient modulus input for base materials into one of three levels. Level-one design input is based on comprehensive laboratory or field determination of the resilient modulus. Level-two design input is based on correlations between resilient modulus and other material strength properties such as California bearing ratio (CBR), R-value, American Association of State Highway and Transportation Officials (AASHTO) structural layer coefficient, or dynamic cone penetrometer index. Level-three design inputs are those estimated by the engineer based on experience and/or the known or estimated soil classification (*1*).

As the MEPDG is gaining popularity with state departments of transportation (DOTs), many DOTs are implementing programs to measure level-one design inputs for their base materials (Sukumaran et al. 2002). However, some DOTs find that direct measurements of resilient modulus are too expensive and time-consuming. These DOTs may prefer instead to correlate resilient modulus to other base material properties that may already be known for many materials within the state or may be easily determined by a standard geotechnical firm (*2*). In particular, the Utah Department of Transportation (UDOT) has fully implemented the MEPDG for pavement design but has been using primarily level-three design inputs obtained from correlations to aggregate base materials developed at the national level (*3*). After developing interest in investigating correlations between laboratory measurements of resilient modulus, CBR, and other material properties specific to base materials commonly used in Utah, UDOT determined that a statewide testing program was needed.

1.2 Research Objectives and Scope

The objectives of this research were to 1) determine the resilient modulus of several representative aggregate base materials in Utah and 2) investigate correlations between laboratory measurements of resilient modulus, CBR, and other properties of the tested materials. The research involved laboratory testing of eight base materials in Utah, two from each of the four UDOT regions. Specifically, the base materials were obtained from the McGuire, Trenton, Beck St., Parley's Canyon, Point of the Mountain, Vernal, Elsinore, and Nielson gravel pits. Each of the eight materials was classified according to AASHTO M 145 (Standard Specification for Classification of Soils and Soil-Aggregate Mixtures for Highway Construction Purposes) and tested according to AASHTO T 307 (Standard Method of Test for Determining the Resilient Modulus of Soil and Aggregate Materials) and American Society for Testing and Materials (ASTM) D1883 (Standard Test Method for CBR (California Bearing Ratio) of Laboratory-Compacted Soils). Relationships between resilient modulus and the other material properties obtained from the laboratory testing were then investigated with the aim of developing correlations specific to aggregate base materials in Utah.

1.3 Outline of Report

This report consists of five chapters. Chapter 1 gives an introduction and explains the objectives and scope of the research. Chapter 2 provides the results of a literature review. Chapter 3 describes the procedures associated with the laboratory testing and statistical analyses. Chapter 4 explains the results. Finally, Chapter 5 includes a summary together with conclusions and recommendations derived from the research.

2.0 BACKGROUND

2.1 Overview

This chapter includes information from the literature about the resilient modulus, particle-size distribution, soil classification, moisture-density relationship, and CBR of aggregate base materials, as well as correlations among these properties.

2.2 Resilient Modulus

The most important material property input for aggregate base materials in the MEPDG is the resilient modulus, and, as explained in Chapter 1, this input can be classified into one of three levels. In laboratory testing, a level-one design input for resilient modulus is obtained using either AASHTO T 307 or National Cooperative Highway Research Program (NCHRP) 1-28A (Laboratory Determination of Resilient Modulus for Flexible Pavement Design). A level-two design input relies on existing correlations between resilient modulus and other commonly used aggregate base material tests, such as CBR, to obtain an estimate of the resilient modulus (*1*). Finally, level-three design inputs are those estimated by the engineer based on experience and/or the known or estimated soil classification (*1*).

Resilient modulus is defined as the ratio of the repeated deviator axial stress to the recoverable axial strain (*1*). Because pavement materials are not purely elastic, they exhibit both recoverable deformation and permanent deformation (*4*). The amount of permanent deformation is largest under the first load cycle and becomes smaller with increasing numbers of cycles (*4*). After the application of a sufficient number of load cycles, the occurrence of permanent deformation is so small that the deformation is almost totally recoverable (*4*). This recoverable deformation is used to calculate the recoverable axial strain, which is used in turn to calculate the resilient modulus as shown in Equations 2-1 and 2-2 (*4*):

$$\varepsilon_r = \frac{\delta_r}{L} \tag{2-1}$$

where:

ε_r = recoverable axial strain (in./in.)
δ_r = recoverable deformation (in.)
L = gauge length (in.)

$$M_r = \frac{\sigma_d}{\varepsilon_r} \quad (2\text{-}2)$$

where:

M_r = resilient modulus (ksi)
σ_d = deviator axial stress (ksi)
ε_r = recoverable axial strain (in./in.)

Determination of the resilient modulus of an aggregate base material using either AASHTO T 307 or NCHRP 1-28A involves application of specific loading cycles intended to simulate repeated traffic loads. Specialized equipment, such as a Universal Testing Machine (UTM) 100 with a confining chamber and servo-hydraulic controls, is required for the testing.

Three principal stresses are applied to the specimen during testing. For cylindrical specimens, the two principal confining stresses are equal to the confining pressure in the confining chamber. The axial stress is equal to the confining stress plus the deviator axial stress. The stress invariant is defined as the sum of the three principal stresses. For a cylindrical sample, the stress invariant is equal to the deviator stress plus three times the confining stress as shown in Equation 2-3:

$$\theta = \sigma_1 + 2\sigma_3 = \sigma_d + 3\sigma_3 \quad (2\text{-}3)$$

where:

θ = stress invariant (ksi)
σ_1 = axial stress (ksi)
σ_3 = confining stress (ksi)
σ_d = deviator axial stress (ksi)

The specimen is subjected to a sequence of combinations of confining stresses and deviator stresses depending on which test procedure is followed. Table 2-1 lists the confining

and deviator stresses to which the specimen is subjected in both AASHTO T 307 and NCHRP 1-28A. Table 2-1 also shows the vertical seating stress that is applied to the specimen during the AASHTO T 307 testing. The resilient modulus and stress invariant are calculated for each loading sequence, and the results for all sequences are plotted together on a log-log graph, with the resilient modulus on the *y*-axis and the stress invariant on the *x*-axis. Least-squares regression is then used to fit a line to the data, with coefficients K_1 and K_2 being calculated as shown in Equation 2-4 (*4*):

$$M_r = K_1\theta^{K_2} \tag{2-4}$$

where:

M_r= resilient modulus (ksi)
θ = stress invariant (ksi)
K_1, K_2 = regression coefficients

As evidenced in Equation 2-4, the resilient modulus increases non-linearly as the stress invariant increases (*4*). The reported resilient modulus is the average of the resilient modulus obtained at each stress invariant. Characterizing an aggregate base material in this manner allows analysis of its mechanical behavior under a variety of loading conditions.

Although a level-one design input for resilient modulus obtained directly from laboratory testing is desirable, this approach is expensive, time-consuming, and complex when compared to other commonly used test procedures such as CBR (*2*). Additionally, resilient modulus testing has proven historically to be less repeatable than other test methods. Although the coefficient of variation (CV) for resilient modulus testing has been shown to be as low as 11 percent for three or more specimens, and as low as 8 percent for two specimens with careful equipment calibration (*5*), a typical CV for resilient modulus testing of granular materials exceeds 15 percent (*5*). Variations in resilient modulus values measured in laboratory testing have been shown to significantly influence the determination of layer thicknesses in the mechanistic-empirical pavement design process (*6*). Determining if laboratory testing is necessary, as opposed to obtaining an estimate from CBR testing, for example, is therefore a matter of weighing the costs of laboratory testing against the benefits of obtaining a direct resilient modulus measurement for a given material.

Table 2-1: Specimen Loading Sequences for Resilient Modulus Testing

	AASHTO T 307			NCHRP 1-28A	
Sequence	Confining Stress (psi)	Deviator Stress (psi)	Seating Stress (psi)	Confining Stress (psi)	Deviator Stress (psi)
0	15.0	15.0	1.5	15.0	30.0
1	3.0	3.0	0.3	3.0	1.5
2	3.0	6.0	0.6	6.0	3.0
3	3.0	9.0	0.9	10.0	5.0
4	5.0	5.0	0.5	15.0	7.5
5	5.0	10.0	1.0	20.0	10.0
6	5.0	15.0	1.5	3.0	3.0
7	10.0	10.0	1.0	6.0	6.0
8	10.0	20.0	2.0	10.0	10.0
9	10.0	30.0	3.0	15.0	15.0
10	15.0	10.0	1.0	20.0	20.0
11	15.0	15.0	1.5	3.0	6.0
12	15.0	30.0	3.0	6.0	12.0
13	20.0	15.0	1.5	10.0	20.0
14	20.0	20.0	2.0	15.0	30.0
15	20.0	40.0	4.0	20.0	40.0
16	-	-	-	3.0	9.0
17	-	-	-	6.0	18.0
18	-	-	-	10.0	30.0
19	-	-	-	15.0	54.0
20	-	-	-	20.0	60.0
21	-	-	-	3.0	15.0
22	-	-	-	6.0	30.0
23	-	-	-	10.0	50.0
24	-	-	-	15.0	75.0
25	-	-	-	20.0	100.0
26	-	-	-	3.0	21.0
27	-	-	-	6.0	2.0
28	-	-	-	10.0	70.0
29	-	-	-	15.0	105.0
30	-	-	-	20.0	140.0

2.3 Particle-Size Distribution

The particle-size distribution of a soil is commonly determined following ASTM C136 (Standard Test Method for Sieve Analysis of Fine and Coarse Aggregates), which yields a percentage by weight of soil finer than each of several standard sieve sizes. The overall particle-size distribution can be quantified by three factors, which include the coefficient of uniformity, the coefficient of curvature, and the fineness modulus. These factors are calculated as shown in Equations 2-5 through 2-7, respectively (*7*):

$$C_u = \frac{D_{60}}{D_{10}} \tag{2-5}$$

where:

C_u = coefficient of uniformity
D_{60} = particle diameter corresponding to 60 percent finer
D_{10} = particle diameter corresponding to 10 percent finer

$$C_c = \frac{{D_{30}}^2}{D_{60} * D_{10}} \tag{2-6}$$

where:

C_c = coefficient of curvature
D_{30} = particle diameter corresponding to 30 percent finer
D_{60} = particle diameter corresponding to 60 percent finer
D_{10} = particle diameter corresponding to 10 percent finer

$$FM = \frac{\sum(Cumulative\ percentage\ retained\ on \frac{3}{8} in., No.8, No.16, No.30, No.50, and\ No.100\ sieves)}{100} \tag{2-7}$$

where:

FM = fineness modulus

The C_u, C_c, and fineness modulus values can be used to compare the particle-size distributions of different materials (*7*).

Past studies have shown that particle-size distribution is a factor that can significantly affect the resilient modulus of granular materials. In general, coarse-grained materials exhibit higher resilient modulus values (*8, 9, 10, 11, 12*), while fine-grained materials exhibit lower resilient modulus values (*9, 11, 13*). Coarse-grained materials exhibit a more rigid structure and therefore a higher resilient modulus than fine-grained materials due to interlocking of the coarse particles (*14*). Although fine particles can provide some support to the soil matrix by minimizing movement of the coarse particles (*15, 16, 17*), increasing amounts of fine particles generally lead to reduced resilient modulus values due to increased disruption of particle-to-particle contact within the coarse aggregate skeleton (*13*).

Particle-size distribution is also closely related to dry density, which has been correlated to resilient modulus for many granular materials (*9, 11, 13, 18, 19, 20*). Well-graded materials typically achieve the highest stiffness, shear strength, and rutting resistance (*18, 21, 22*).

2.4 Soil Classification

Soil properties such as particle-size distribution and plasticity index (PI) can be used to classify a soil according to its potential suitability as an aggregate base material. The PI of a soil is determined as the difference between the plastic and liquid limits of a soil, which are measured according to ASTM D4318 (Standard Test Methods for Liquid Limit, Plastic Limit, and Plasticity Index of Soils). Whereas the particle-size distribution can be used to assess the amount of fines in a soil, the PI is used to determine the quality of the fines.

Soil classification is performed using either the AASHTO system or the Unified Soil Classification System (USCS). The AASHTO system, which is described in AASHTO M 145, classifies an aggregate base material into one of seven major categories, with the A-1-a classification indicating an excellent to good aggregate base material. In the USCS, which is described in ASTM D2487 (Standard Practice for Classification of Soils for Engineering Purposes (Unified Soil Classification System)), a soil is classified as gravel, sand, silt, clay, or organic, with supplemental designations given to indicate poorly-graded or well-graded materials or to indicate high or low plasticity.

Although less important than particle-size distribution, PI can also affect the resilient modulus of a soil in certain situations. While several researchers have not found PI to be a significant factor affecting the resilient modulus of aggregate base materials (*23*, *24*), other researchers have found that the resilient modulus of base materials increases with increasing PI of the fines when the PI values are comparatively low (*25*, *26*, *27*). In the MEPDG, the PI is used in conjunction with the percentage of fines passing the No. 200 sieve to predict resilient modulus values of base materials (*1*).

2.5 Moisture-Density Relationship

The maximum dry density (MDD) of a soil is the density of the dry soil after compaction at the optimum moisture content (OMC) and is determined for many aggregate base materials following the procedures outlined in ASTM D1557 (Standard Test Methods for Laboratory Compaction Characteristics of Soil Using Modified Effort (56,000 ft-lbf/ft^3 (2,700 kN-m/m^3))). While the MDD is constant for a particular material and compaction effort, the density of the soil is affected by the water content at the time of compaction; specifically, the density of the soil increases with increasing water content below OMC and decreases with increasing water content above OMC. The density of a soil reaches the MDD when the water content at the time of compaction is equal to the OMC.

Knowledge of both the OMC and MDD is important in laboratory testing to determine resilient modulus values for aggregate base materials (*28*), as testing at the MDD, or at a specified percentage of the MDD, is commonly recommended. Deviations from MDD can lead to predictable changes in the resilient modulus of a given aggregate base material type; however, variations in resilient modulus across different material types are not necessarily correlated to differences in MDD (*27*) due, at minimum, to possible differences in specific gravity of the different aggregate types.

2.6 California Bearing Ratio

The CBR of a given soil is defined as the bearing capacity of that soil relative to that of a standard crushed rock (*4*). As described in ASTM D1883, the CBR test is performed by pushing

a piston with a 2-in.-diameter circular face into the surface of a compacted soil specimen at a constant strain rate of 0.05 in./minute. The load required to drive the piston into the soil is recorded at 0.1-in. penetration depth intervals to a maximum penetration depth of 0.5 in. Determining the CBR value involves calculating the bearing stress from the load recorded at each penetration depth interval and dividing the resulting bearing stresses by standard values given in ASTM D1883, which are shown in Table 2-2. The highest ratio is multiplied by 100 and reported as the CBR for the tested soil.

Because CBR is affected by many of the same factors that affect resilient modulus, such as the degree of particle-to-particle contact within the coarse aggregate skeleton, materials with higher CBR values can also have higher resilient modulus values (*1, 29, 30*). However, due to the fundamental differences in the loading conditions applied in the two tests and also the variable non-linear behavior between different material types, CBR and resilient modulus values may not be well correlated for some individual materials or for some groups of materials (*12, 31*). In some cases, improved estimations of resilient modulus using CBR can be achieved by also accounting for variability in other soil properties, such as shear strength (*32*).

Table 2-2: Standard Stresses for California Bearing Ratio Calculations

Penetration Depth (in.)	Standard Stress (psi)
0.1	1000
0.2	1500
0.3	1900
0.4	2300
0.5	2600

2.7 Existing Correlations

Due to the complexity of the testing required for laboratory determination of resilient modulus, researchers have studied correlations between resilient modulus and aspects of particle-size distribution, soil classification, MDD, and CBR, which can all be measured relatively easily using standard laboratory equipment. Several correlations published in the literature are presented in the following Equations 2-8 through 2-14. In each case, correlation with the

average resilient modulus should be assumed rather than correlation with the resilient modulus measured at a particular stress invariant.

The MEPDG suggests a correlation between CBR and resilient modulus as shown in Equation 2-8 (*1*):

$$M_r = 2555(CBR)^{0.64} \quad (2\text{-}8)$$

where:

M_r= resilient modulus (psi)
CBR = California bearing ratio (%)

A relationship between the resilient modulus and CBR of in-situ materials was determined from the U.S. Army Corps of Engineers as shown in Equation 2-9 (*29*):

$$M_r = 1500 * CBR \quad (2\text{-}9)$$

where:

M_r= resilient modulus (psi)
CBR = California bearing ratio (%)

Resilient modulus was also correlated to CBR by the Georgia DOT for some fine-grained subgrade soils as shown in Equation 2-10 (*30*):

$$M_r = 3116 * CBR^{0.4779707} \quad (2\text{-}10)$$

where:

M_r= resilient modulus (psi)
CBR = California bearing ratio (%)

When an estimate of CBR is needed for Equations 2-8 through 2-10, values can be obtained through correlations to aspects of the particle-size distribution and PI of the soil as shown in Equations 2-11 and 2-12 (*1*):

$$CBR = 28.09 * {D_{60}}^{0.358} \quad (2\text{-}11)$$

where:

CBR = California bearing ratio (%)
D_{60} = particle size corresponding to 60 percent passing (mm)

$$CBR = \frac{75}{(1+0.728*P_{200}*PI)} \quad (2\text{-}12)$$

where:

CBR = California bearing ratio (%)
P_{200}= percent passing the No. 200 sieve (%)
PI= plasticity index

Resilient modulus has also been correlated directly with selected soil properties. For example, resilient modulus values obtained from the Highway Research Information Service database have been correlated to moisture content, bulk stress, and soil classification for coarse-grained soils as shown in Equation 2-13 (*23*):

$$\log M_r = 0.523 - 0.025 * w_c + 0.544 * \log\theta + 0.173 * SM + 0.197 * GR \quad (2\text{-}13)$$

where:

M_r= resilient modulus (ksi)
w_c = gravimetric moisture content (%)
θ = stress invariant (psi)
SM = 1 for SM soils classified using USCS
= 0 otherwise
GR = 1 for GM, GW, GC, or GP soils classified using USCS
= 0 otherwise

The resilient modulus values of 12 coarse-grained soils in Mississippi were correlated to the dry density, moisture content, percent passing the No. 200 sieve, and coefficient of uniformity as shown in Equation 2-14 (*27*):

$$M_r = 307.4 * \left(\frac{\gamma_{dr}}{w_c}\right)^{0.86} * \left(\frac{P_{200}}{\log C_u}\right)^{-0.46} \quad (2\text{-}14)$$

where:

M_r= resilient modulus (MPa)
γ_{dr} = ratio of dry density to MDD, expressed as a fraction
w_c = gravimetric moisture content (%)
P_{200}= percent passing the No. 200 sieve
C_u = coefficient of uniformity

In addition to equations, tables have also been developed to show correlations among resilient modulus, CBR, and soil classification as presented in the MEPDG (*1*, *33*). Table 2-3 shows the results of laboratory resilient modulus tests on soils having different AASHTO or Unified soil classifications; the data in Table 2-3 are average resilient modulus values measured at the respective OMC and MDD values for the given soils (*33*). Table 2-4 shows resilient modulus values determined in the MEPDG using Equation 2-8, with CBR values being estimated using Equation 2-11 from particle-size distribution ranges specified in the AASHTO system and USCS for the indicated materials.

These correlations describe relationships between resilient modulus, CBR, and selected soil properties for the specific soils for which the equations were developed. As of yet, no study has been conducted that focuses specifically on UDOT base materials. As a result, UDOT engineers have been assuming resilient modulus values of 40 and 38 ksi for A-1-a and A-1-b aggregates, respectively, as recommended in Table 2-3 (*33*).

Table 2-3: Measured Resilient Modulus Values by Soil Classification

AASHTO or Unified Soil Classification	Resilient Modulus Range (psi)	Typical Resilient Modulus (psi)
A-1-a	38,500-42,000	40,000
A-1-b	35,500-40,000	38,000
A-2-4	28,000-37,500	32,000
A-2-5	24,000-33,000	28,000
A-2-6	21,500-31,000	26,000
A-2-7	21,500-28,000	24,000
A-3	24,500-35,500	29,000
A-4	21,500-29,000	24,000
A-5	17,000-25,500	20,000
A-6	13,500-24,000	17,000
A-7-5	8,000-17,500	12,000
A-7-6	5,000-13,500	8,000
CH	5,000-13,500	8,000
MH	8,000-17,500	11,500
CL	13,500-24,000	17,000
ML	17,000-25,000	20,000
SW	28,000-37,000	32,000
SP	24,000-33,000	28,000
SW-SC	21,500-31,000	25,500
SW-SM	24,000-33,000	28,000
SP-SC	21,500-31,000	25,500
SP-SM	24,000-33,000	28,000
SC	21,500-28,000	24,000
SM	28,000-37,500	32,000
GW	39,500-42,000	41,000
GP	35,500-40,000	38,000
GW-GC	28,000-40,000	34,500
GW-GM	35,500-40,500	38,500
GP-GC	28,000-39,000	34,000
GP-GM	31,000-40,000	36,000
GC	24,000-37,500	31,000
GM	33,000-42,000	38,500

Table 2-4: Estimated California Bearing Ratio and Resilient Modulus Values by Soil Classification

AASHTO or Unified Soil Classification	Typical CBR Range	Resilient Modulus Range (psi)	Typical Resilient Modulus (psi)
A-1-a	60-80	30,000-42,000	38,000
A-1-b	35-60	25,000-35,000	29,000
A-2-4	20-40	17,000-28,000	21,000
A-2-5	15-30	14,000-22,000	17,000
A-2-6	10-25	12,000-20,000	15,000
A-2-7	10-20	12,000-17,000	14,000
A-3	15-35	14,000-25,000	18,000
A-4	10-20	12,000-18,000	14,000
A-5	8-16	9,000-15,000	11,000
A-6	5-15	7,000-14,000	9,000
A-7-5	2-8	4,000-9,500	6,000
A-7-6	1-5	2,500-7,000	4,000
CH	1-5	2,500-7,000	4,000
MH	2-8	4,000-9,500	6,000
CL	5-15	7,000-14,000	9,000
ML	8-16	9,000-15,000	11,000
SW	20-40	17,000-28,000	21,000
SP	15-30	14,000-22,000	17,000
SW-SC	10-25	12,000-20,000	15,000
SW-SM	15-30	14,000-22,000	17,000
SP-SC	10-25	12,000-20,000	15,000
SP-SM	15-30	14,000-22,000	17,000
SC	10-20	12,000-17,000	14,000
SM	20-40	17,000-28,000	21,000
GW	60-80	35,000-42,000	38,000
GP	35-60	25,000-35,000	29,000
GW-GC	20-60	17,000-35,000	24,000
GW-GM	35-70	25,000-38,000	30,000
GP-GC	20-50	17,000-32,000	23,000
GP-GM	25-60	20,000-35,000	26,000
GC	15-40	14,000-28,000	20,000
GM	30-80	22,000-42,000	30,000

2.8 Summary

The most important material property input for aggregate base materials in the MEPDG is the resilient modulus. Although a design input for resilient modulus obtained directly from laboratory testing is desirable, testing using either AASTHO T 307 or NCHRP 1-28A is complex. Therefore, researchers have studied correlations between resilient modulus and aspects of particle-size distribution, soil classification, MDD, and CBR, which can all be measured relatively easily using standard laboratory equipment. Soil properties such as particle-size distribution and PI can be used to classify a soil according to its potential suitability as an aggregate base material. Past studies have shown that particle-size distribution is a factor that can significantly affect the resilient modulus of granular materials. Although less important than particle-size distribution, PI can also affect the resilient modulus of a soil in certain situations. Knowledge of both the OMC and MDD is important in laboratory testing to determine resilient modulus values for aggregate base materials, as testing at the MDD, or at a specified percentage of the MDD, is commonly recommended. Because CBR is affected by many of the same factors that affect resilient modulus, such as the degree of particle-to-particle contact within the coarse aggregate skeleton, materials with higher CBR values can also have higher resilient modulus values.

Several correlation equations relating particle-size distribution, soil classification, MDD, and CBR to resilient modulus have been published in the literature. Tables have also been developed to show correlations among resilient modulus, CBR, and soil classification as presented in the MEPDG. These correlations describe relationships between resilient modulus, CBR, and selected soil properties for the specific soils for which the equations were developed. As of yet, no study has been conducted that focuses specifically on UDOT base materials.

3.0 PROCEDURES

3.1 Overview

This chapter explains the material sampling process and the procedures used to determine the particle-size distribution, soil classification, moisture-density relationship, CBR, and resilient modulus for each of the tested materials. In addition, the statistical analyses performed in this research are described.

3.2 Material Sampling

Two aggregate base materials were obtained from each of the four UDOT regions as recommended by the respective UDOT region materials and pavement engineers. Table 3-1 lists each material by the name of the respective aggregate pit from which it was obtained, and Figure 3-1 depicts the distribution of the sampling locations across the state of Utah. The materials were sampled in general accordance with ASTM D75 (Standard Practice for Sampling Aggregates). The Trenton and Nielson materials were sampled directly from active pavement

Table 3-1: Aggregate Base Materials Selected for Testing

UDOT Region	Material	Company	Pit Address or Coordinates
1	McGuire	Staker Parson Companies	8211 S Highway 89 Willard, UT 84340
	Trenton	Trenton Gravel Pit No. 3	N 41.905201, W 111.956642
2	Beck St.	Staker Parson Companies	1730 North Beck Street, Salt Lake City, UT 84116
	Parley's Canyon	Kilgore Companies	1 Parley's Canyon, Salt Lake City, UT 84102
3	Point of the Mountain	Staker Parson Companies	12800 West SR 73, Lehi, UT 84043
	Vernal	Burdick Materials	Maeser East Pit, Highway 121, Vernal UT 84078
4	Elsinore	Staker Parson Companies	180 W 1400 S Elsinore, UT 84724
	Nielson	Nielson Construction	39.103140, -111.156539

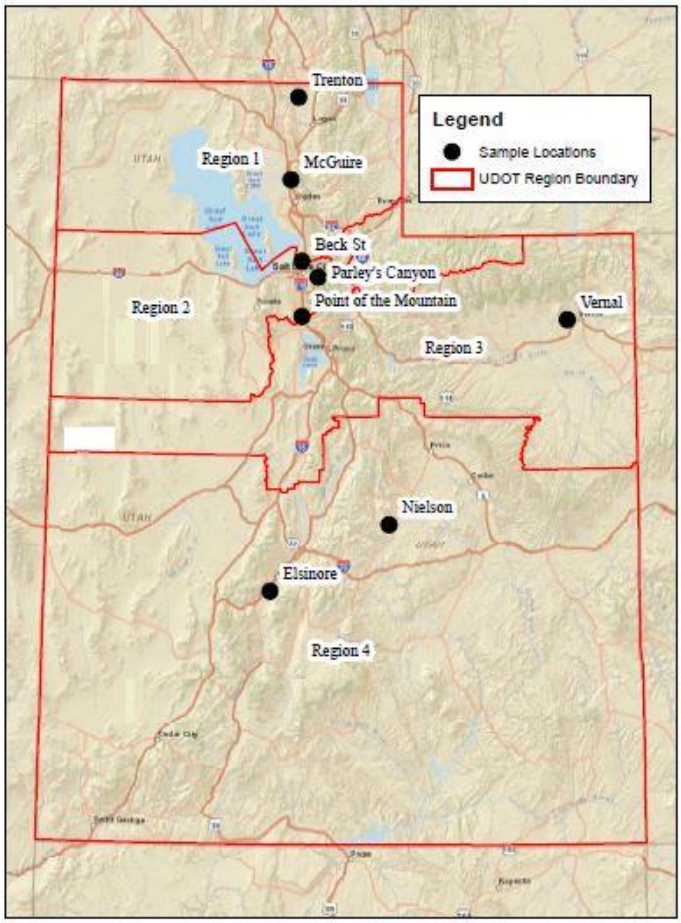

Figure 3-1: Aggregate base material sampling locations.

construction projects, while the remaining six materials were sampled directly from the source pits; in the former cases, the materials were sampled from the grade prior to compaction, while in the latter cases a front-end loader was used to scoop a large amount of material from the stockpile and spread it on the floor of the gravel pit for sampling. The aggregate samples were manually loaded into 5-gallon buckets using shovels and transported to the Brigham Young University Highway Materials Laboratory for testing.

3.3 Material Characterization

Important material properties, including particle-size distribution, soil classification, and the moisture-density relationship were investigated for each of the sampled aggregate base materials. The following sections outline the laboratory procedures associated with this testing.

3.3.1 Particle-Size Distribution and Soil Classification

The aggregate base materials were classified using the AASHTO system in general accordance with AASHTO M 145. The AASHTO method for classifying soils is based primarily on particle-size distribution and PI.

The particle-size distribution of the soil was determined in general accordance with ASTM D6913 (Standard Test Methods for Particle-Size Distribution (Gradation) of Soils Using Sieve Analysis). Upon delivery to the laboratory, each aggregate base material sample was dried in an oven at 230°F for at least 24 hours. Each material was then separated across the 3/4 in., 1/2 in., 3/8 in., No. 4, No. 8, No. 16, No. 30, No. 50, No. 100, and No. 200 sieve sizes. The materials retained on the different sieve sizes were placed in different containers for storage. The total weight of each material retained on each sieve was recorded, and the percent by dry weight of material retained on each sieve size was then calculated as a basis for preparing samples with the same particle-size distributions for further testing.

A washed sieve analysis was then performed in general accordance with ASTM C136. For each aggregate, a 5-lb sample was prepared following the previously prepared particle-size distribution. Each sample was washed over the same set of sieves used in the earlier sieve analysis, and the material retained on each sieve size was dried in the oven at 140°F for at least 24 hours until reaching constant weight. The material was then weighed, and the percent by dry weight of material retained on each sieve size was then calculated as the basis for classifying each material. The fineness modulus of each material was also calculated from the results of the washed sieve analysis using Equation 2-7.

The PI for each material was determined in general accordance with ASTM D4318. A representative 5-lb sample of each material passing the No. 40 sieve was prepared for this testing. If a plastic limit could not be determined, then the material was determined to be non-plastic. If the material was plastic, the liquid limit test was performed. For materials for which a plastic limit could be determined, the PI was determined as the difference between the plastic limit and the liquid limit. Once the washed particle-size distributions and PIs were measured, the AASHTO soil classifications were determined.

3.3.2 Moisture-Density Relationship

The OMC and MDD were determined from the moisture-density relationship for each aggregate base material in general accordance with ASTM D1557. Three to five specimens of each material were prepared for this testing. In each case, the amounts of each sieve size necessary to produce a specimen 4.0 in. in diameter and 4.59 in. in height were weighed out according to the results of the particle-size analysis performed on the bulk material. The aggregates were then oven-dried at 230°F for at least 24 hours to remove any residual moisture that may have accumulated in the material during storage. After being removed from the oven and allowed to cool to room temperature, the dried aggregates were then moistened at target gravimetric moisture contents ranging between 4.0 and 8.0 percent by weight of dry aggregate. An additional 0.5 percent of water was added to each specimen to compensate for the amount of water evaporation typically observed during the remaining procedures.

The specimens were then compacted into a steel mold using an automated compaction machine, with 25 blows of a 10-lb hammer applied to each of five lifts per specimen. The sample surface was scarified between lifts, and three blows of a finishing tool were applied to the top of the final lift to flatten the surface of the sample. The weights and heights of the specimens were measured after compaction, and the specimens were then extruded and oven-dried at 140°F for at least 48 hours. The resulting dry weights of the specimens were used together with the previously measured weights and heights to compute the moisture content and dry density of each specimen. For each aggregate, the dry density measurements were then plotted against the corresponding moisture content measurements, an approximately parabolic curve was fit to the data, and the OMC and MDD were estimated graphically.

3.4 California Bearing Ratio Testing

The CBR of each aggregate base material was tested in general accordance with ASTM D1883. The following sections describe specimen preparation, specimen testing, and data analysis procedures for this testing.

3.4.1 Specimen Preparation

Two or three specimens of each material were prepared for CBR testing. In each case, the amounts of each sieve size necessary to produce a specimen 6.0 in. in diameter and 4.59 in. in height were weighed out according to the results of the particle-size analysis performed on the bulk material. The aggregates were then oven-dried at 230°F for at least 24 hours to remove any residual moisture that may have accumulated in the material during storage. After being removed from the oven and allowed to cool to room temperature, the dried aggregates were then moistened at the respective OMC values, and an additional 0.5 percent of water was added to each specimen to compensate for the amount of water evaporation typically observed during the remaining procedures. The specimens were then compacted into a steel mold using an automated compaction machine, with 56 blows of a 10-lb hammer applied to each of five lifts per specimen. The sample surface was scarified between lifts, and three blows of a finishing tool were applied to the top of the final lift to flatten the surface of the sample. The weights and heights of the specimens were measured after compaction, and the specimens, still in their molds, were then sealed in airtight plastic bags and allowed to equilibrate at room temperature for approximately 24 hours.

3.4.2 Specimen Testing

After the equilibration period, the CBR of each specimen was measured. As shown in Figures 3-2 and 3-3, a metal collar was placed on top of the tested specimen to provide the required overburden stress, and the loading piston was driven into the top surface of the specimen at a rate of 0.05 in./minute. During the testing, the penetration of the piston into the specimen surface was measured, and the applied load was recorded on 0.1-in. intervals from 0.1 to 0.5 in. of penetration. After the testing, the specimens were extruded from the molds and oven-dried at 140°F for at least 48 hours. The resulting dry weights of the specimens were used together with the previously measured weights and heights to compute the moisture content and dry density of each specimen.

Figure 3-2: California bearing ratio specimen.

Figure 3-3: California bearing ratio testing.

3.4.3 Data Analysis

In the analysis of the CBR data, the applied stress was determined for each 0.1-in. penetration interval using Equation 3-1:

$$\sigma_x = \frac{P_x}{A} \tag{3-1}$$

where:

σ_x = stress at deflection interval x
P_x= load at deflection interval x
A = area of the loading piston = 3.0 in.^{2}

The stresses computed at the specified intervals were divided by the standard stresses listed in ASTM D1883, which are duplicated in Table 2-2, to obtain the ratio of the measured stress to the standard stress at the same deflection. The maximum of these ratios was multiplied by 100 to obtain the CBR for the given specimen.

3.5 Resilient Modulus Testing

The resilient modulus of each aggregate base material was tested in general accordance with AASHTO T 307. The following sections describe specimen preparation, specimen testing, and data analysis procedures for this testing.

3.5.1 Specimen Preparation

Three to five specimens of each material were prepared for resilient modulus testing. In each case, the amounts of each sieve size necessary to produce a specimen 6.0 in. in diameter and 12.0 in. in height were weighed out according to the results of the particle-size analysis performed on the bulk material. The aggregates were then oven-dried at 230°F for at least 24 hours to remove any residual moisture that may have accumulated in the material during storage. After being removed from the oven and allowed to cool to room temperature, the dried aggregates were then moistened at the respective OMC values, and an additional 0.5 percent of water was added to each specimen to compensate for the amount of water evaporation typically observed during the remaining procedures. A hinged steel split mold was lined on the inside

with a rubber membrane, and a steel collar was placed on top of the mold and over the membrane to protect the membrane from damage during the compaction process. The specimens were then compacted into the mold using a manual compaction hammer, with 56 blows of a 10-lb hammer applied to each of five lifts per specimen. Figure 3-4 shows the empty split mold, and Figure 3-5 shows the compaction process. The sample surface was scarified between lifts, and three blows of a finishing tool were applied to the top of the final lift to flatten the surface of the sample. The weights and heights of each specimen were measured after compaction, and the specimen was then removed from the mold. An outer membrane was placed around the outside of the specimen, which was then sealed in airtight plastic bags and allowed to equilibrate at room temperature for 24 hours.

The specimens were then prepared for placement inside the confining chamber. Following the removal of the specimen from the split mold, the specimens were placed on top of an approximately 0.25-in.-thick porous stone, and the specimens and porous stones were then placed on top of a 6-in.-diameter metal platen integral with the bottom of the confining chamber. A drain hole located in the center of the platen allowed the specimens to drain freely during testing; Figure 3-6 shows the drainage line that conveyed water from the platen through the bottom of the confining chamber. Another platen with a semi-spherical indent in the center was placed on top of the specimens; the indent served as the receptacle of the loading rod during testing. As shown in Figure 3-7, the ends of both membranes were extended beyond the outer faces of the platens, and rubber o-rings were then placed over the membranes around the circumference of the platens to seal the interface between the membranes and platens.

After the specimen was prepared, the top of the confining chamber was installed, and the entire assembly was placed inside the environmental chamber of the testing machine, as shown in Figure 3-8. Two linear variable differential transformers were positioned at the top of the confining chamber to measure the deflection of the specimen during testing, as depicted in Figure 3-9. A pressure transducer was used to measure the air pressure inside the confining chamber.

Figure 3-4: Split mold for resilient modulus specimen preparation.

Figure 3-5: Compaction of resilient modulus specimen.

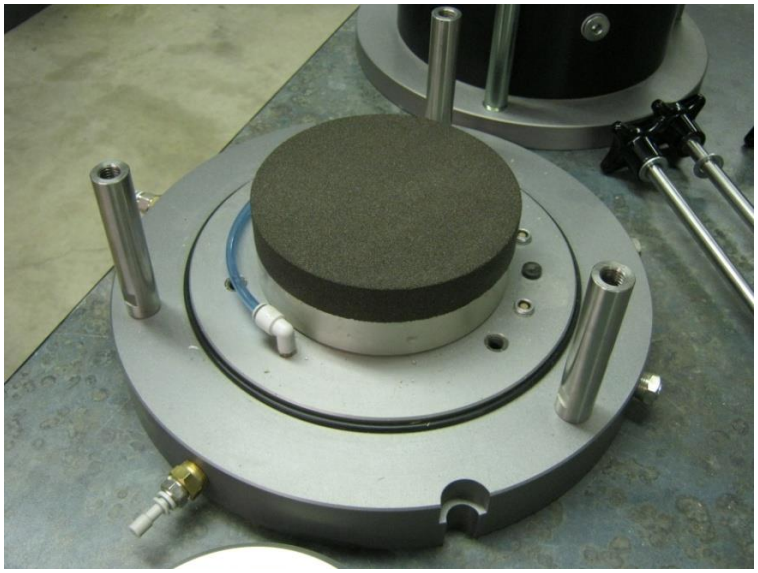

Figure 3-6: Base of confining chamber for resilient modulus testing.

Figure 3-7: Membranes around resilient modulus specimen.

Figure 3-8: Resilient modulus specimen in confining chamber.

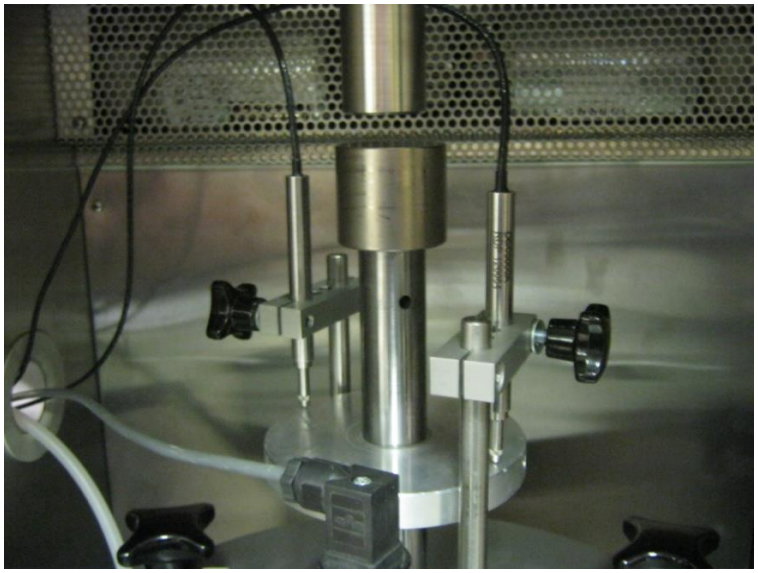

Figure 3-9: Linear variable differential transformers for resilient modulus testing.

3.5.2 Specimen Testing

The specimens were tested in 15 different loading sequences of deviatoric stress and confining pressure as listed in Table 2-1. The deviatoric stress, confining stress, resilient deformation, and permanent deformation were recorded for the final five cycles of each loading sequence. The specimen testing was terminated if the permanent deformation exceeded 5 percent of the specimen height, as per AASHTO T 307. After the testing, the specimens were removed from the confining chamber, the o-rings and membranes were removed from the specimens. The specimens were then divided into approximately thirds and weighed, and each part was oven-dried at 140°F for at least 24 hours. The resulting dry weights were used to compute the moisture content of each sample, and a weighted average moisture content for the entire specimen was used together with the previously measured weights and heights to compute the dry density of each specimen.

3.5.3 Data Analysis

After testing, the resilient modulus values of the specimens were calculated. The recoverable strain for each sequence was computed as shown in Equation 2-1, and the resilient modulus was then determined as the average of the resilient modulus values calculated as shown in Equation 2-2 for each sequence.

3.6 Statistical Analysis

After all of the data were collected, the applicable equations presented in Chapter 2 were evaluated to determine if one or more of those existing models could be used to predict the resilient modulus values measured in this research. A plot of the predicted and measured values for all eight of the aggregate base materials was then prepared for each model, and the *p*-value and coefficient of determination, or R^2 value, for a regression line fit through the data were used to evaluate the suitability of the model in each case. Models with low *p*-values, preferably less than or equal to 0.15, and high R^2 values were desired (*34*).

Additional statistical analyses were performed to investigate correlations between measurements of resilient modulus, CBR, and other properties of the tested aggregate base

materials, mainly including aspects of the particle-size distributions and moisture-density relationships determined in this research. Specifically, the percentages passing the 0.5-in., 0.375-in., No. 4, No. 8, No. 16, No. 50, No. 100, and No. 200 sieves; particle sizes corresponding to 10, 30, and 60 percent finer; coefficient of uniformity; coefficient of curvature; fineness modulus; OMC; MDD; and CBR were included in the analyses as possible predictor variables for resilient modulus.

In the initial analyses, correlations among the predictor variables were identified, and selected predictor variables were removed from consideration in order to obtain a set of independent predictor variables. The set of independent predictor variables was then analyzed using both stepwise regression and best subset analysis to develop a new model for predicting resilient modulus. In stepwise regression, variables were selected for inclusion in the model if the computed *p*-values were less than or equal to 0.15, which is the default value for variable selection in many statistical software programs. For best subset analysis, subsets of the predictor variables were selected based on the computed Mallows' Cp value, where a Mallows' Cp value that is close to the number of predictors plus the constant indicates that the model is relatively unbiased in estimating the true regression coefficients and predicting responses (*35*). In both cases, potential models were also evaluated based on the computed R^2 value.

After a suitable model was developed, it was analyzed to determine the sensitivity of the regression coefficients and intercept to the individual data points. For each iteration in this sensitivity analysis, one of the eight data points was systematically removed from the analysis, and the regression coefficients and intercept were recomputed using the seven remaining data points. The new model was then used to predict the resilient modulus of the excluded point. The error was determined as the difference between the predicted and measured resilient modulus values. The root mean squared error (RMSE) was determined for all of the errors from the eight iterations of the sensitivity analysis. A low RMSE indicated a robust model.

3.7 Summary

Two aggregate base materials were obtained from each of the four UDOT regions as recommended by the respective UDOT region materials and pavement engineers. The materials

were sampled in general accordance with ASTM D75. Important material properties, including particle-size distribution, soil classification, and the moisture-density relationship were investigated for each of the sampled aggregate base materials.

The CBR of each aggregate base material was tested in general accordance with ASTM D1883. Two or three specimens of each material were prepared for CBR testing. The specimens were compacted at OMC into steel molds and then allowed to equilibrate in plastic bags at room temperature for approximately 24 hours. During the testing, the penetration of the piston into the specimen surface was measured, and the applied load was recorded on 0.1-in. intervals from 0.1 to 0.5 in. of penetration. The stresses computed at the specified intervals were divided by the standard stresses listed in ASTM D1883 to obtain the ratio of the measured stress to the standard stress at the same deflection. The maximum of these ratios was multiplied by 100 to obtain the CBR for the given specimen. After the testing, the moisture content of the specimens was obtained, and the dry density of the specimen was calculated.

The resilient modulus of each aggregate base material was tested in general accordance with AASHTO T 307. Three to five specimens of each material were prepared for resilient modulus testing. The specimens were compacted at OMC into a hinged steel split mold with a rubber membrane liner and then allowed to equilibrate in plastic bags at room temperature for approximately 24 hours. An additional rubber membrane liner was then placed around the specimen. The specimen was placed into a confining chamber, and a UTM 100 was used to load the specimen in predetermined loading sequences. For each sequence, the resilient modulus was calculated as the average of the last five loading cycles. After the testing, the moisture content of the specimens was obtained, and the dry density of the specimen was calculated.

After all of the data were collected, the applicable equations presented in Chapter 2 were evaluated to determine if one or more of those existing models could be used to predict the resilient modulus values measured in this research. Statistical analyses were also performed to investigate correlations between measurements of resilient modulus, CBR, and other properties of the tested aggregate base materials, mainly including aspects of the particle-size distributions and moisture-density relationships determined in this research. A set of independent predictor variables was analyzed using both stepwise regression and best subset analysis to develop a new

model for predicting resilient modulus. After a suitable model was developed, it was analyzed to determine the sensitivity of the model coefficients to the individual data points.

4.0 RESULTS

4.1 Overview

The following sections present the results of material characterization, CBR testing, resilient modulus testing, and statistical analysis.

4.2 Material Characterization

The results of material characterization include sieve analyses, plastic and liquid limit determinations, PIs, AASHTO soil classifications, and moisture-density relationships for the tested aggregates. The results of the washed sieve analyses are listed in Table 4-1, which also lists the fineness modulus determined for each material. Plots of the particle-size distributions resulting from the washed sieve analyses are presented in Appendix A.

With the exception of the Parley's Canyon material, which was determined to have a plastic limit of 14.1 percent, the materials tested in this study were determined to be non-plastic. The liquid limit and PI of the Parley's Canyon material were determined to be 15.3 percent and 1.2, respectively. Since the other materials were determined to be non-plastic, the liquid limit and PI were not measured.

The results of the AASHTO soil classification were based on the particle-size distributions obtained from the washed sieve analysis and the PI testing. The AASHTO soil classification is A-1-a for every material, suggesting that each material is well suited as a base material.

The results of moisture-density testing for each material are listed in Table 4-2. The OMC varies from 5.4 percent for the Nielson material to 6.6 percent for the Vernal material, while the MDD varies from 137.4 pcf for the Point of the Mountain and Elsinore materials to 145.0 pcf for the Beck St. material. The moisture-density curves for each material are presented in Appendix B.

Table 4-1: Results of Washed Sieve Analyses

Material	Percent by Weight Passing Indicated Sieve Size (%)									Fineness Modulus
	1/2 in.	3/8 in.	No. 4	No. 8	No. 16	No. 30	No. 50	No. 100	No. 200	
McGuire	77.8	66.5	46.9	36.0	28.0	17.9	10.8	6.9	5.0	3.3
Trenton	83.7	70.7	48.6	36.7	26.7	18.9	11.8	6.1	4.8	3.7
Beck St.	87.0	80.8	54.1	36.7	27.3	22.1	17.9	14.5	11.3	3.5
Parley's Canyon	96.2	87.9	62.5	43.8	32.1	24.4	19.0	15.5	13.3	3.9
Point of the Mountain	92.8	87.1	62.3	41.3	30.0	24.5	14.3	11.7	7.2	3.8
Vernal	83.3	71.8	50.9	39.3	32.0	27.0	21.9	14.8	10.2	3.3
Elsinore	80.9	70.4	51.3	38.2	29.0	20.9	11.4	7.0	5.0	3.4
Nielson	83.8	76.3	58.4	40.6	30.5	18.5	10.8	6.7	5.4	3.5

Table 4-2: Results of Moisture-Density Testing

Material	OMC (%)	MDD (pcf)
McGuire	5.8	139.3
Trenton	5.6	142.2
Beck St.	6.3	145.0
Parley's Canyon	6.1	143.0
Point of the Mountain	6.4	137.4
Vernal	6.6	140.3
Elsinore	6.3	137.4
Nielson	5.4	138.6

4.3 California Bearing Ratio Testing

The results of CBR testing are shown in Table 4-3. The average CBR varies from 18 percent for the Vernal material to 109 percent for the Point of the Mountain material. A summary of the results for each specimen is provided in Appendix C.

Table 4-3: Results of California Bearing Ratio Testing

UDOT Region	Material	CBR (%)	
		Average	St. Dev.
1	McGuire	94	11.1
	Trenton	60	25.1
2	Beck St.	52	2.5
	Parley's Canyon	33	11.8
3	Point of the Mountain	109	2.8
	Vernal	18	1.7
4	Elsinore	93	27.8
	Nielson	82	7.8

4.4 Resilient Modulus Testing

The results of resilient modulus testing are shown in Table 4-4. The average resilient modulus varies from 16.0 ksi for the Point of the Mountain material to 25.6 ksi for the Nielson material. Based on Equation 2-4, the average K_1 value ranges from 1,298 for the Elsinore

Table 4-4: Results of Resilient Modulus Testing

UDOT Region	Material	Resilient Modulus (ksi)		K_1		K_2	
		Average	St. Dev.	Average	St. Dev.	Average	St. Dev.
1	McGuire	20.2	2.9	1311	419	0.706	0.110
	Trenton	22.4	4.5	1975	405	0.621	0.098
2	Beck St.	20.9	2.5	2890	291	0.512	0.044
	Parley's Canyon	21.3	0.9	2199	332	0.588	0.044
3	Point of the Mountain	16.0	0.5	1643	489	0.596	0.091
	Vernal	20.5	1.4	2309	462	0.566	0.063
4	Elsinore	18.7	3.8	1298	286	0.683	0.049
	Nielson	25.6	8.8	2205	707	0.626	0.015

material to 2,890 for the Beck St. material, while the average K_2 value ranges from 0.512 for the Beck St. material to 0.706 for the McGuire material. A summary of the results for each specimen and plots of resilient modulus values and stress invariants are provided in Appendix D.

4.5 Statistical Analysis

The plots prepared to determine if one or more of the existing models presented in Chapter 2 could be used to predict the resilient modulus values measured in this research are shown in Figures 4-1 through 4-5. These plots depict the relationships between the measured values and those predicted using Equations 2-8, 2-9, 2-10, 2-13, and 2-14, respectively. Each data point in the plots represents one of the eight aggregate base materials tested in this research, and the diagonal line in each plot is the line of equality. For Equation 2-13, a stress invariant of 48 psi was assumed in the calculations.

The *p*-value and R^2 value provided in Table 4-5 for each model indicate that especially Equations 2-8, 2-9, 2-10, and 2-14 are not suitable for predicting the resilient modulus of aggregate base materials in Utah. In all four of these cases, the *p*-value is well above the specified threshold of 0.15, and the R^2 value is well below 1.0. Regarding Equation 2-13, while the *p*-value is lower than 0.15, the R^2 value is still comparatively low. Therefore, none of the existing models was determined to be satisfactory for predicting the resilient modulus of aggregate base materials in Utah.

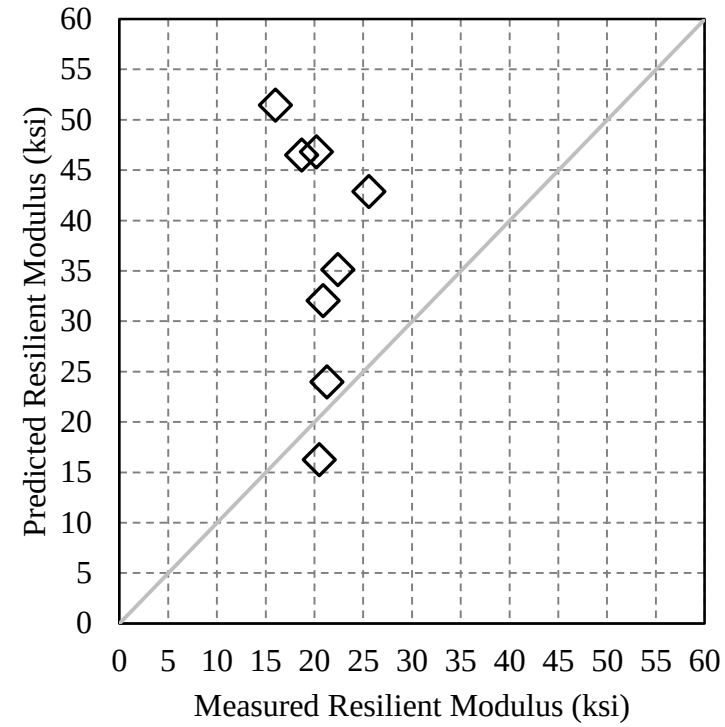

Figure 4-1: Predicted and measured resilient modulus values for Equation 2-8.

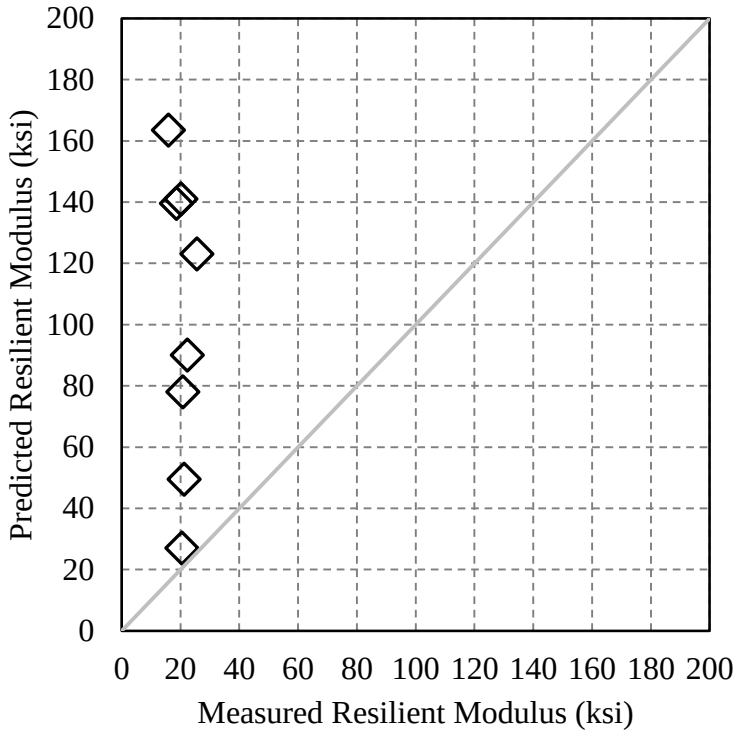

Figure 4-2: Predicted and measured resilient modulus values for Equation 2-9.

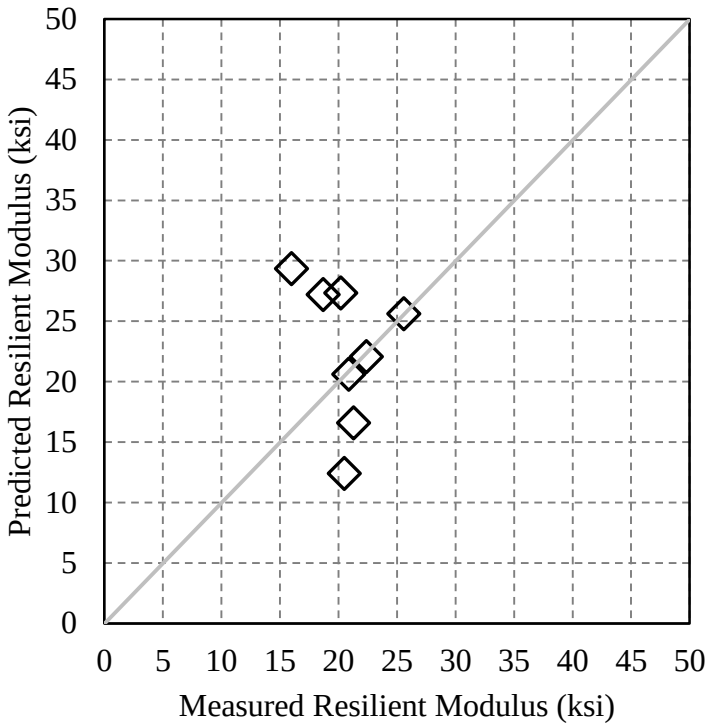

Figure 4-3: Predicted and measured resilient modulus values for Equation 2-10.

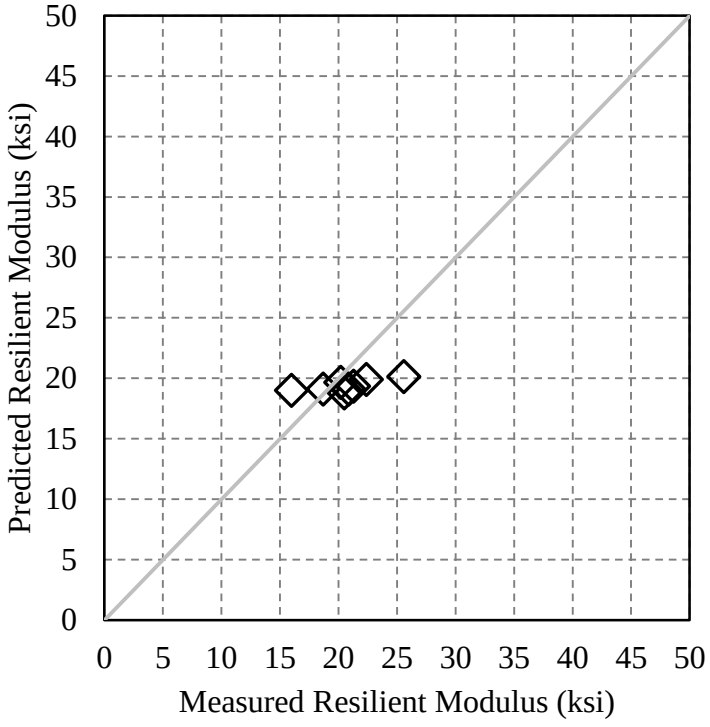

Figure 4-4: Predicted and measured resilient modulus values for Equation 2-13.

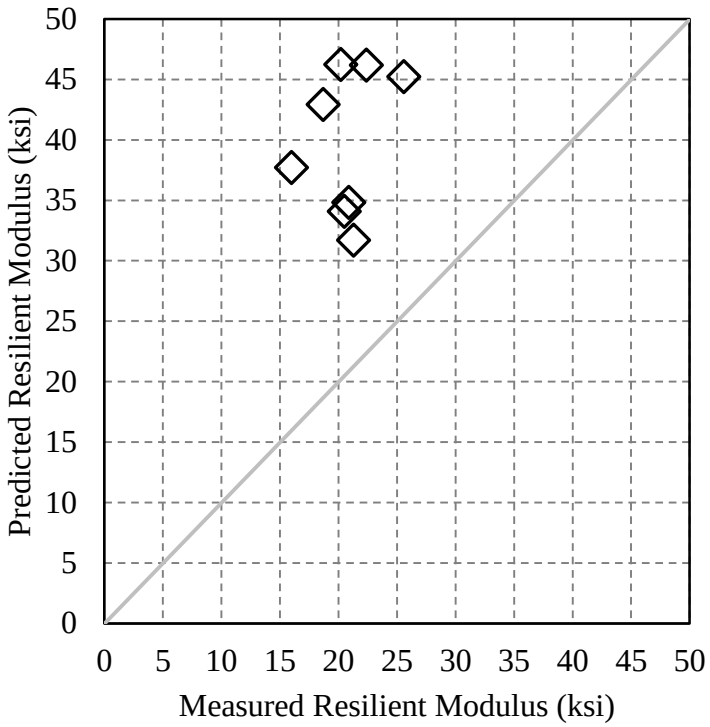

Figure 4-5: Predicted and measured resilient modulus values for Equation 2-14.

The discrepancies between the measured and predicted values may be attributable to variations in soil properties between those used to develop the models and those of the aggregate base materials tested in this research and/or to lack of applicability of the models to the ranges of values examined in this research. For example, Equation 2-9 provides the most accurate estimates of resilient modulus when the CBR of the soil is less than about 20 (*4*) and therefore, as demonstrated in this research, may not provide accurate estimates for aggregate base materials with high CBR values. As with all empirically derived equations, limitations inherent in these

Table 4-5: Summary of Fitness Parameters for Existing Models

Model	*p*-Value	R^2 Value
Equation 2-8	0.475	0.088
Equation 2-9	0.402	0.119
Equation 2-10	0.509	0.076
Equation 2-13	0.036	0.546
Equation 2-14	0.492	0.082

models lead to boundaries on their appropriate applications, and the results of this research should therefore not be viewed as discrediting these models in general.

For development of a new model, correlations between laboratory measurements of resilient modulus, CBR, and other properties of the tested materials were evaluated. In particular, the correlation analysis indicated that resilient modulus and CBR are not correlated for the materials tested in this research; a correlation analysis between these two properties yielded a *p*-value of 0.402 and an R^2 value of 0.119. In an additional correlation analysis, the average resilient modulus and average CBR for each material were adjusted to account for variations in the dry density of these specimens; specifically, the average resilient modulus and average CBR were divided by the respective average relative density of the test specimens, which was computed as the ratio of dry density to MDD; however, this approach yielded only a slightly improved *p*-value of 0.394 and an R^2 value of 0.123, again indicating a lack of correlation.

Therefore, given the absence of a correlation between resilient modulus and CBR, correlations between resilient modulus and other material properties were investigated. In this analysis, the average resilient modulus for each material was also divided by the average relative density of the test specimens to account for variations in the dry density of the specimens. The analysis, for which the complete statistical output is presented in Appendix E, yielded the following Equation 4-1:

$$M_r = (-200 - 1.51 * P_{200} - 418 * D_{30} - 3.09 * OMC + 1.94 * MDD) * \gamma_{dr} \qquad (4\text{-}1)$$

where:

M_r = resilient modulus (ksi)
P_{200} = percent passing the No. 200 sieve (%)
D_{30} = particle diameter corresponding to 30 percent finer (in.)
OMC = optimum moisture content (%)
MDD = maximum dry density (pcf)
γ_{dr} = ratio of dry density to MDD, expressed as a fraction

The *p*-values for all of the predictor variables in Equation 4-1 are well below 0.15 as desired, the Mallows' Cp value is optimum at 5.0, and the R^2 value for this model is high at

0.968, indicating that only 3.2 percent of the variability in resilient modulus is not explained by variability in the predictor variables. Figure 4-6 depicts the relationship between the measured values and those predicted using Equation 4-1. As with the previous plots, each data point in the plot represents one of the eight aggregate base materials tested in this research, and the diagonal line in the plot is the line of equality. Table 4-6 lists the ranges of the predictor variables used to develop Equation 4-1. The equation may not be applicable for values outside the specified ranges of the given properties.

The results of the sensitivity analysis performed on the new model developed in this research are given in Table 4-7, which lists the regression coefficients and intercept computed in each iteration of the analysis together with those determined for the model including all aggregate base materials, as presented in Equation 4-1. Table 4-7 also lists the difference between the predicted and measured resilient modulus values for each iteration. The maximum difference between the measured and predicted values is comparatively low at 3.2 ksi, and the RMSE for all the iterations was only 1.7 ksi. These data indicate that the model is not overly dependent on a single data point and is therefore satisfactorily robust. The complete statistical output for these analyses is given in Appendix E.

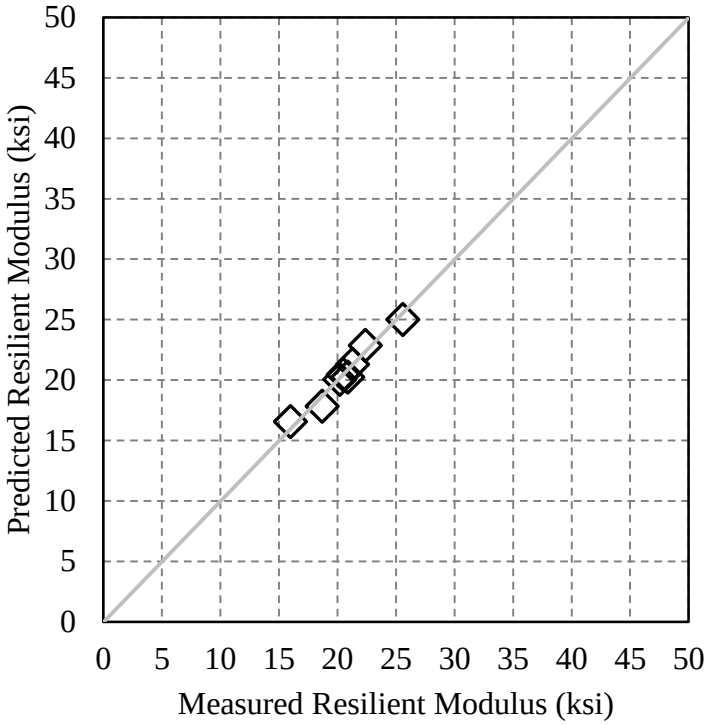

Figure 4-6: Predicted and measured resilient modulus values for Equation 4-1.

Table 4-6: Ranges of Predictor Variables Used in Development of New Model

Property	Minimum	Maximum
Resilient Modulus (ksi)	16.0	25.6
Percent Passing the No. 200 Sieve (%)	4.8	13.3
Particle Diameter Corresponding to 30 Percent Finer (in.)	0.0376	0.0651
Optimum Moisture Content (%)	5.4	6.6
Maximum Dry Density (pcf)	137.4	145.0

Table 4-7: Results of Sensitivity Analysis for New Model

		Regression Coefficients for Indicated Variable				Values for Excluded Material		
Model	*y*-Intercept	P_{200}	D_{30}	OMC	MDD	Predicted	Measured	Error
Including All Materials	-200	-1.51	-418	-3.09	1.94	-	-	-
Excluding McGuire	-200	-1.51	-418	-3.09	1.94	20.4	20.2	-0.2
Excluding Trenton	-258	-1.92	-469	-2.62	2.38	25.6	22.4	-3.2
Excluding Beck St.	-197	-1.64	-467	-3.31	1.96	18.7	20.9	2.2
Excluding Parley's Canyon	-189	-1.40	-410	-3.46	1.87	22.1	21.3	-0.8
Excluding Point of the Mountain	-148	-1.20	-349	-3.28	1.54	17.4	16	-1.4
Excluding Vernal	-243	-1.81	-493	-2.15	2.25	21.6	20.5	-1.1
Excluding Elsinore	-203	-1.47	-425	-3.57	1.98	17.5	18.7	1.2
Excluding Nielson	-206	-1.47	-384	-2.12	1.93	23.9	25.6	1.7
Maximum	-148	-1.20	-349	-2.12	2.38	-	-	2.2
Minimum	-258	-1.92	-493	-3.57	1.54	-	-	-3.2

4.6 Summary

The results of material characterization, CBR testing, resilient modulus testing, and statistical analysis are presented. The results of material characterization include sieve analyses, plastic and liquid limit determinations, PIs, AASHTO soil classifications, and moisture-density relationships for the tested aggregates. With the exception of the Parley's Canyon material, which was determined to have a plastic limit of 14.1 percent, the materials used in this study were determined to be non-plastic. The AASHTO soil classification is A-1-a for every material, suggesting that each material is well suited as a base material. The OMC varies from 5.4 percent for the Nielson material to 6.6 percent for the Vernal material, while the MDD varies from 137.4 pcf for the Point of the Mountain and Elsinore materials to 145.0 pcf for the Beck St. material.

The results of CBR testing and resilient modulus testing are also presented. The average CBR varies from 18 percent for the Vernal material to 109 percent for the Point of the Mountain material. The average resilient modulus varies from 16.0 ksi for the Point of the Mountain material to 25.6 ksi for the Nielson material. Based on Equation 2-4, the average K_1 value ranges from 1,298 for the Elsinore material to 2,890 for the Beck St. material, while the average K_2 value ranges from 0.512 for the Beck St. material to 0.706 for the McGuire material.

The results of the statistical analysis indicate that especially Equations 2-8, 2-9, 2-10, and 2-14 are not suitable for predicting the resilient modulus of aggregate base materials in Utah. The discrepancies between the measured and predicted values may be attributable to variations in soil properties between those used to develop the models and those of the aggregate base materials tested in this research and/or to lack of applicability of the models to the ranges of values examined in this research. Therefore, a new model was needed.

For development of a new model, correlations between laboratory measurements of resilient modulus, CBR, and other properties of the tested materials were evaluated. In particular, the correlation analysis indicated that resilient modulus and CBR are not correlated for the materials tested in this research, even when the average resilient modulus and average CBR for each material were adjusted to account for variations in the dry density of these specimens. Therefore, a model was developed as shown in Equation 4-1 to predict the resilient modulus from the percent passing the No. 200 sieve, particle diameter corresponding to 30

percent finer, OMC, MDD, and ratio of dry density to MDD. The *p*-values for all of the predictor variables in Equation 4-1 are well below 0.15 as desired, the Mallows' Cp value is optimum at 5.0, and the R^2 value for this model is high at 0.968. The equation may not be applicable for values outside the ranges of the predictor variables used to develop it. The results of the sensitivity analysis performed on the new model indicated that the model is not overly dependent on a single data point and is therefore satisfactorily robust.

5.0 CONCLUSION

5.1 Summary

UDOT has fully implemented the MEPDG for pavement design but has been using primarily level-three design inputs obtained from correlations to aggregate base materials developed at the national level. After developing interest in investigating correlations between laboratory measurements of resilient modulus, CBR, and other material properties specific to base materials commonly used in Utah, UDOT determined that a statewide testing program was needed. The objectives of this research were to 1) determine the resilient modulus of several representative aggregate base materials in Utah and 2) investigate correlations between laboratory measurements of resilient modulus, CBR, and other properties of the tested materials.

Two aggregate base materials were obtained from each of the four UDOT regions as recommended by the respective UDOT region materials and pavement engineers. The materials were sampled in general accordance with ASTM D75. Important material properties, including particle-size distribution, soil classification, and the moisture-density relationship were investigated for each of the sampled aggregate base materials. The CBR and resilient modulus of each aggregate base material were determined in general accordance with ASTM D1883 and AASHTO T 307, respectively. In both cases, specimens of each material were tested at OMC.

After all of the data were collected, the applicable equations presented in Chapter 2 were evaluated to determine if one or more of those existing models could be used to predict the resilient modulus values measured in this research. Statistical analyses were also performed to investigate correlations between measurements of resilient modulus, CBR, and other properties of the tested aggregate base materials, mainly including aspects of the particle-size distributions and moisture-density relationships. A set of independent predictor variables was analyzed using both stepwise regression and best subset analysis to develop a model for predicting resilient modulus. After a suitable model was developed, it was analyzed to determine the sensitivity of the model coefficients to the individual data points.

5.2 Conclusions

A few conclusions corresponding to the research objectives can be derived from this work. For the tested aggregate base materials, the average resilient modulus varied from 16.0 ksi for the Point of the Mountain material to 25.6 ksi for the Nielson material. To the extent that these materials are similar to others used by UDOT, resilient modulus values in this range may therefore be expected. Because direct measurements of resilient modulus are expensive and time-consuming, UDOT may prefer to correlate resilient modulus to other base material properties that may already be known for many materials within the state or may be easily determined by a standard geotechnical firm.

The results of the statistical analysis indicate that the resilient modulus values measured for the eight aggregate base materials tested in this research cannot be satisfactorily predicted by any of the existing models. The discrepancies between the measured and predicted values may be attributable to variations in soil properties between those used to develop the models and those of the aggregate base materials tested in this research and/or to lack of applicability of the models to the ranges of values examined in this research. In addition, the correlation analysis indicated that resilient modulus and CBR are not correlated for the materials tested in this research, even when the average resilient modulus and average CBR for each material were adjusted to account for variations in the dry density of these specimens. Therefore, a new model was developed as shown in Equation 4-1 to predict the resilient modulus based on the percent passing the No. 200 sieve, particle diameter corresponding to 30 percent finer, OMC, MDD, and ratio of dry density to MDD. Although the equation may not be applicable for values outside the ranges of the predictor variables used to develop it, it is expected to provide UDOT with reasonable estimates of resilient modulus values for aggregate base materials similar to those tested in this research.

5.3 Recommendations

Ideally, when sufficient funding and time are available, laboratory testing of multiple specimens is recommended to determine average resilient modulus values of aggregate base materials. As additional resilient modulus testing is performed, measurement of the percent

passing the No. 200 sieve, particle diameter corresponding to 30 percent finer, OMC, MDD, and dry density of test specimens is recommended to allow evaluation of the applicability of the model developed in this research to other aggregates.

When resilient modulus values obtained from laboratory testing are not readily available, use of the model developed in this research is recommended, provided that the values used in the equation are within the specified ranges. Because the model inputs can all be readily obtained from basic information about the particle-size distribution and moisture-density relationship for a given aggregate base material, the model is easy to implement in standard practice. In the absence of any laboratory data, use of an average resilient modulus value of 20.0 ksi may be appropriate for A-1-a materials similar to those studied in this research. Use of correlations involving CBR is not recommended, as resilient modulus and CBR are not correlated for the materials tested in this research.

REFERENCES

1. ERES Consultants. (2004). *Guide for Mechanistic-Empirical Pavement Design of New and Rehabilitated Pavement Structures,* Report 1-37A, National Cooperative Highway Research Program, Federal Highway Administration, Washington, DC.

2. Sukumaran, B., Kyatham, V., Shah, A., and Sheth, D. (2002). "Suitability of Using California Bearing Ratio Test to Predict Resilient Modulus," *Proceedings of the Federal Aviation Administration Airport Technology Transfer Conference,* Galloway, NJ.

3. Darter, M. I., Leslie, T., and Von Quintus, H. L. (2009). *Implementation of the Mechanistic-Empirical Pavement Design Guide in Utah: Validation, Calibration, and Development of the UDOT MEPDG User's Guide,* Report No. UT-09.11, Utah Department of Transportation, Salt Lake City, UT.

4. Huang, Y. H. (2004). *Pavement Analysis and Design*, 2nd Ed., Upper Saddle River, NJ.

5. Barksdale, R. D., Jorge, A., Khosla, N. P., Kim, K., Lambe, P.C., and Rahman, M.S. (1998). *Laboratory Determination of Resilient Modulus for Flexible Pavement Design*, Report 1-28, National Cooperative Highway Research Program, Federal Highway Administration, Washington, DC.

6. Andrei, D., Witczak, M., Schwartz, C., and Uzan, J. (2004). *Harmonized Resilient Modulus Test Method for Unbound Pavement Materials,* Report 1-28A, National Cooperative Highway Research Program, Federal Highway Administration, Washington, DC.

7. Daas, B. (2011). *Principles of Foundation Engineering*, 7th Ed., Cengage Learning, Stamford CT.

8. Kirkpatrick, W. M. (1965). "Effects of Grain Size and Grading on the Shearing Behaviour of Granular Materials," *Proceedings of the 6th International Conference on Soil Mechanics and Foundation Engineering,* University of Toronto, Montreal, Quebec, 1, 273-277.

9. Lekarp, F., Isacsson, U., and Dawson, A. (2000). "State of the Art. I: Resilient Response of Unbound Aggregates," *Journal of Transportation Engineering*, 126(1), 66-75.

10. Leslie, D. (1963). "Large Scale Triaxial Tests on Gravelly Soils," *Proceedings of the 2nd Panamerican Conference on Soil Mechanics and Foundation Engineering*, Rio de Janeiro, Brazil, 1, 181-202.

11. Tian, P., Zaman, M., and Laguros, J. (1998). "Gradation and Moisture Effects on Resilient Moduli of Aggregate Bases," *Transportation Research Record: Journal of the Transportation Research Board*, 1619, 75-84.

12. Zaman, M., Chen, D., and Laquros, J. (1994). "Resilient Moduli of Granular Materials," *Journal of Transportation Engineering*, 120(6), 967–988.

13. Hicks, R. G., and Monismith, C. L. (1971). "Factors Influencing the Resilient Response of Granular Materials," *Highway Research Record*, 345, 15-31.

14. Cunningham, C. N., Evans, T. M., and Tayebali, A. A. (2013). "Gradation Effects on the Mechanical Response of Crushed Stone Aggregate," *International Journal of Pavement Engineering*, 14(3), 231-241.

15. Knight, J. A. (1935). "Gradation of Aggregate as Applied to Stabilization of Gravel Roads," *Canadian Engineer*, 13(23), 9-10.

16. Radjai, F., Wolf, D. E., Jean, M., and Moreau, J. J. (1998). "Bimodal Character of Stress Transmission in Granular Packings," *Physical Review Letters*, 80(1), 61-64.

17. Voivret, C., Radjai, F., Delenne, J.-Y., and El Youssoufi, M. S. (2009). "Multiscale Force Networks in Highly Polydisperse Granular Media," *Physical Review Letters*, 102(17), Article 178001, 1-4.

18. Barksdale, R. D., and Itani, S. Y. (1989). "Influence of Aggregate Shape on Base Behavior," *Transportation Research Record: Journal of the Transportation Research Board*, 1227, 173-182.

19. Rada, G., and Witczak, M. W. (1982). "Material Layer Coefficients of Unbound Granular Materials from Resilient Modulus," *Transportation Research Record: Journal of the Transportation Research Board*, 852, 15-21.

20. Zeghal, M. (2000). "Variability of Resilient Moduli of Aggregate Materials Due to Different Gradations," *Proceedings of the Canadian Society for Civil Engineering Annual Conference, National Research Council Canada Institute for Research in Construction*, London, Ontario, 363-367.

21. Brown, S. F., and Chan, F. W. K. (1996). "Reduced Rutting in Unbound Granular Pavement Layers through Improved Grading Design," *Proceedings of the Institution of Civil Engineers: Transport*, 117(1), 40-49.

22. Thom, N. H., and Brown, S. F. (1988). "The Effect of Grading and Density on the Mechanical Properties of a Crushed Dolomitic Limestone," *Proceedings of the 14th Australian Road Research Board Conference*, Canberra, Australia, 14(7), 94-100.

23. Carmichael, III, R. F., and Stuart, E. (1978). "Predicting Resilient Modulus: A Study to Determine the Mechanical Properties of Subgrade Soils," *Transportation Research Record: Journal of the Transportation Research Board*, 1043, 20-28.

24. Rahim, A. M. (2005). "Subgrade Soil Index Properties to Estimate Resilient Modulus for Pavement Design," *International Journal of Pavement Engineering*, 6(3), 163-169.

25. Drumm, E., Boateng-Poku, Y., and Johnson Pierce, T. (1990). "Estimation of Subgrade Resilient Modulus from Standard Tests," *Journal of Geotechnical Engineering*, 116(5), 774-789.

26. Farrar, M. J., and Turner, J. P. (1991). *Resilient Modulus of Wyoming Subgrade Soils*, Report No. 91-1, Mountain Plains Consortium, University of Wyoming, Laramie, WY.

27. George, K. P. (2004). *Resilient Modulus Prediction Employing Soil Index Properties*, Report No. FHWA/MS-DOT-RD-04-172, Mississippi Department of Transportation, Jackson, MS.

28. Amber, Y., and H. L. Von Quintus. (2002). *Study of LTPP Laboratory Resilient Modulus Test Data and Response Characteristics*, Report FHWA-RD-02-051, Federal Highway Administration, Washington, DC.

29. Heukelom, W., and Klomp, A J. G. (1962). "Dynamic Testing as a Means of Controlling Pavements during and after Construction," *Proceedings of the First International Conference on Structural Design of Asphalt Pavements*, University of Michigan, Ann Arbor, MI.

30. Webb, W. M., and Campbell, B. E. (1986). "Preliminary Investigation into Resilient Modulus Testing for New AASHTO Pavement Design Guide," Office of Materials and Research, Georgia Department of Transportation, Atlanta, GA.

31. Figueroa, J. L., and Thompson, M. R. (1980). "Simplified Structural Analysis of Flexible Pavements for Secondary Roads Based on ILLI-PAVE," *Transportation Research Record: Journal of the Transportation Research Board*, 776, 17-23.

32. Kyalham, V., and Willis, M. (2001). "Predictive Equations for Determination of Resilient Modulus, Suitability of Using California Bearing Ratio Test to Predict Resilient Modulus," *Proceedings of the Federal Aviation Administration Airport Technology Transfer Conference*, Galloway, NJ.

33. Utah Department of Transportation (UDOT). (2012). *UDOT Pavement Design Manual of Instruction*, Utah Department of Transportation, Salt Lake City, UT.

34. Ramsey, F., and Schafer, D. (2013). *The Statistical Sleuth: A Course in Methods of Data Analysis,* 3rd Ed., Brooks/Cole, Cengage Learning, Boston, MA.

35. Minitab, Inc. (2015). "What is Mallows' Cp?" <http://support.minitab.com/en-us/minitab/17/topic-library/modeling-statistics/regression-and-correlation/goodness-of-fit-statistics/what-is-mallows-cp/> (Nov. 19, 2015).

APPENDIX A PARTICLE-SIZE DISTRIBUTIONS

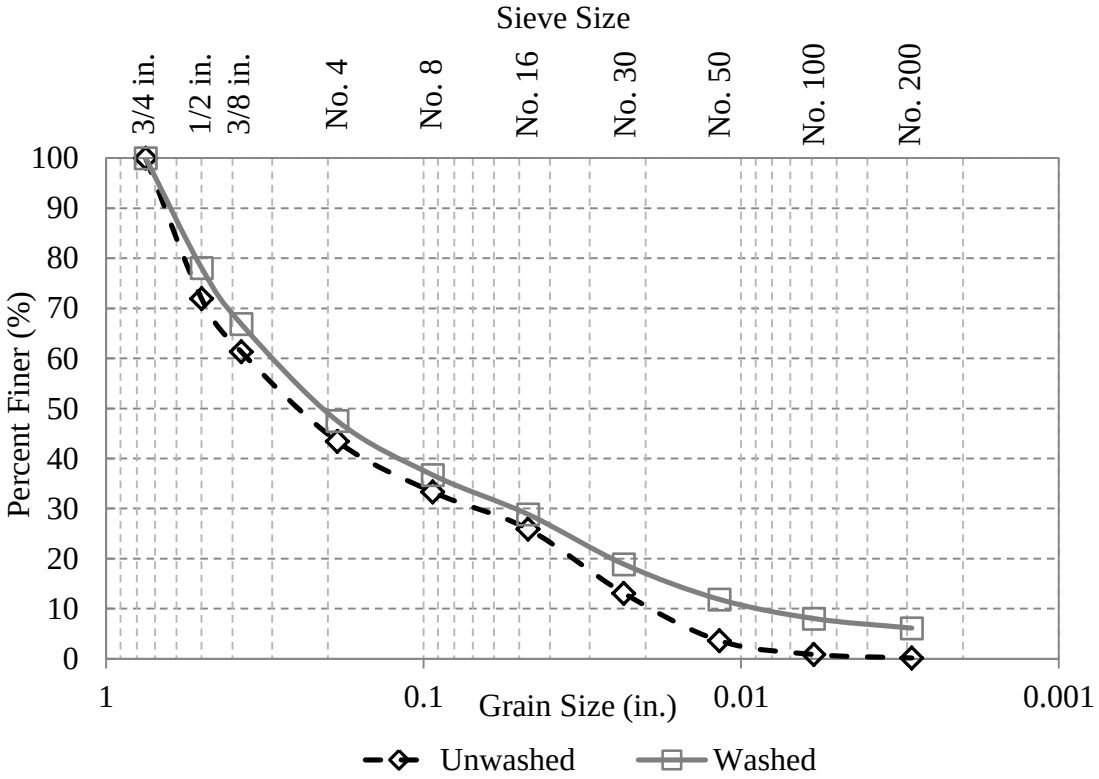

Figure A-1: Particle-size distribution for McGuire material.

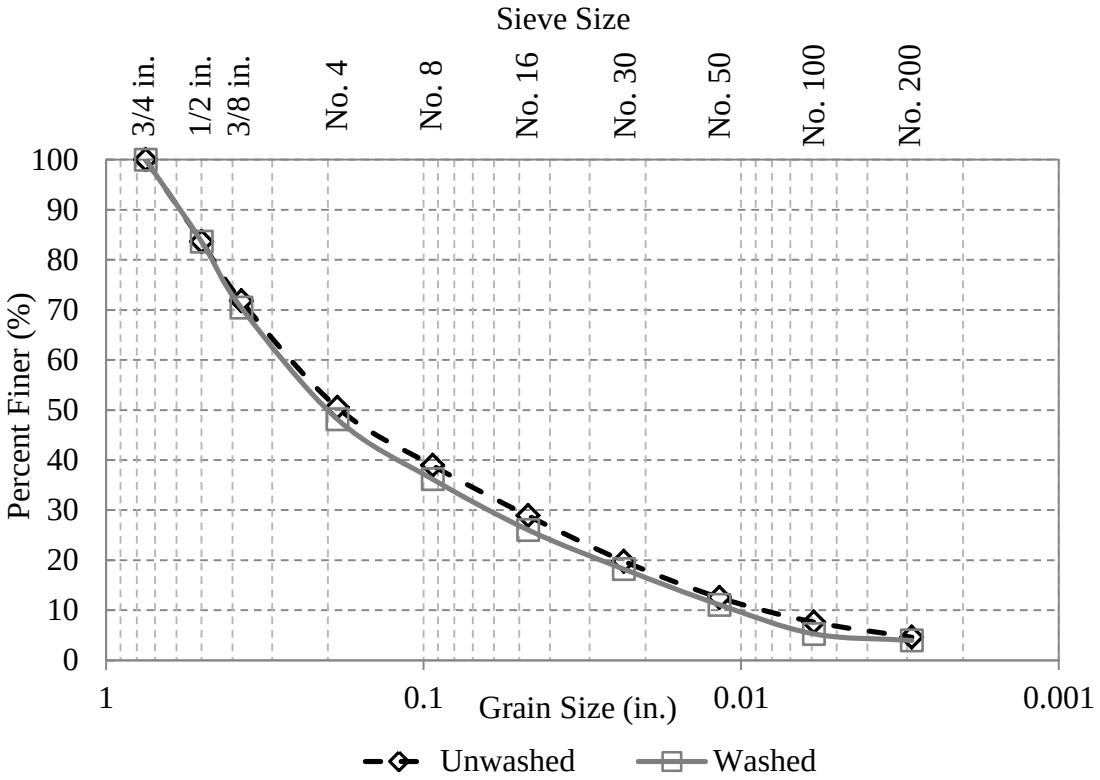

Figure A-2: Particle-size distribution for Trenton material.

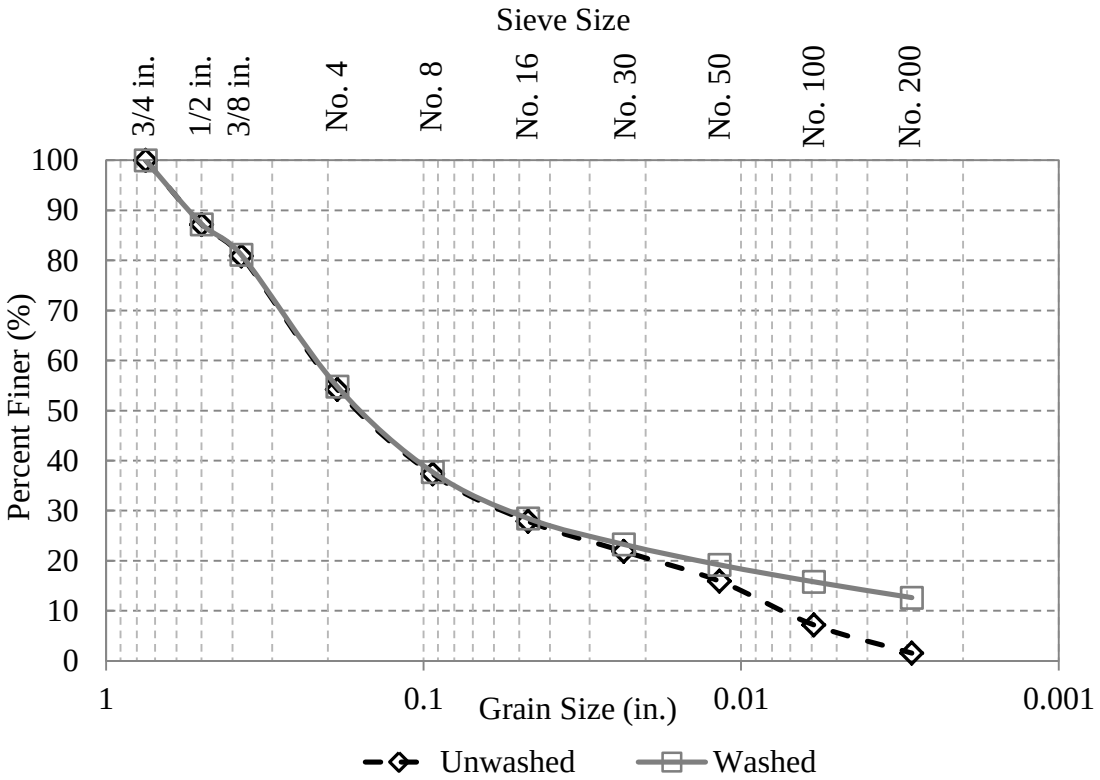

Figure A-3: Particle-size distribution for Beck St. material.

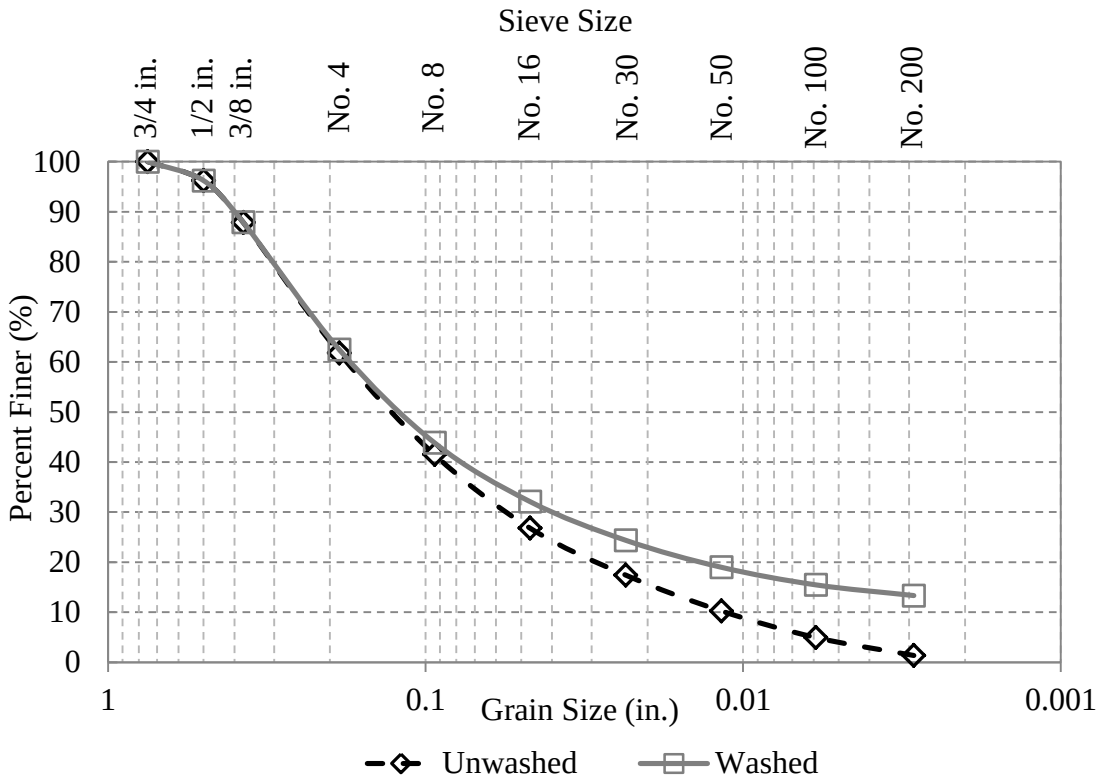

Figure A-4: Particle-size distribution for Parley's Canyon material.

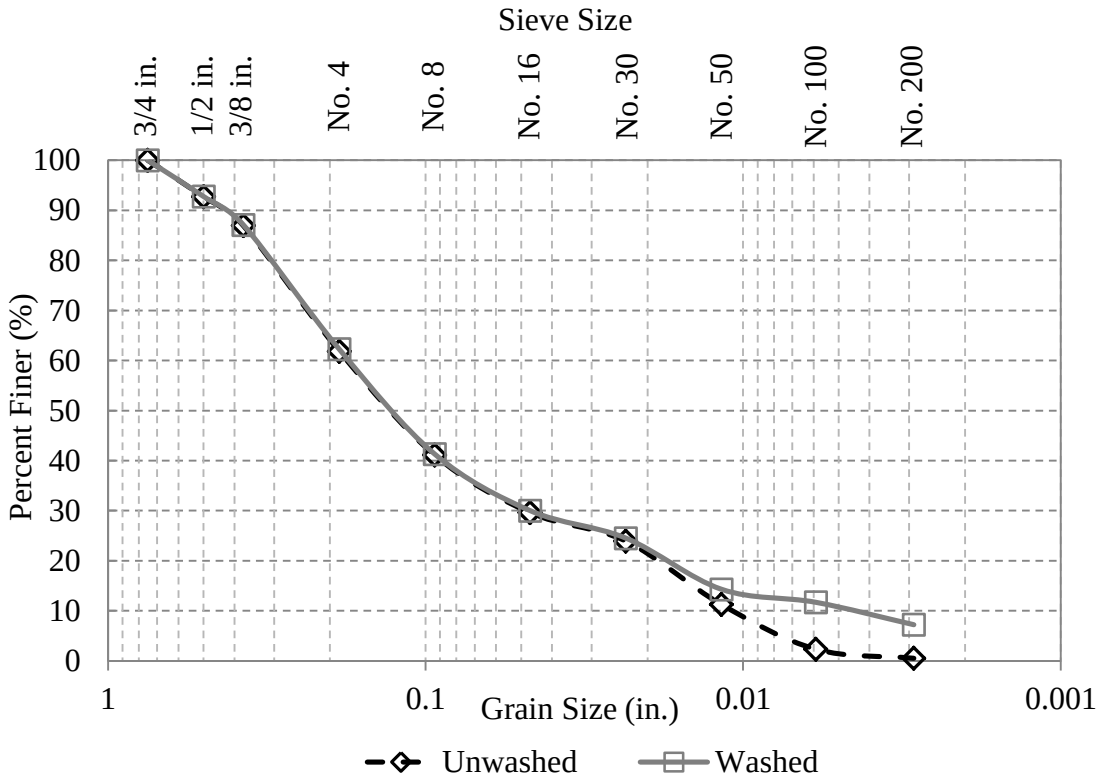

Figure A-5: Particle-size distribution for Point of the Mountain material.

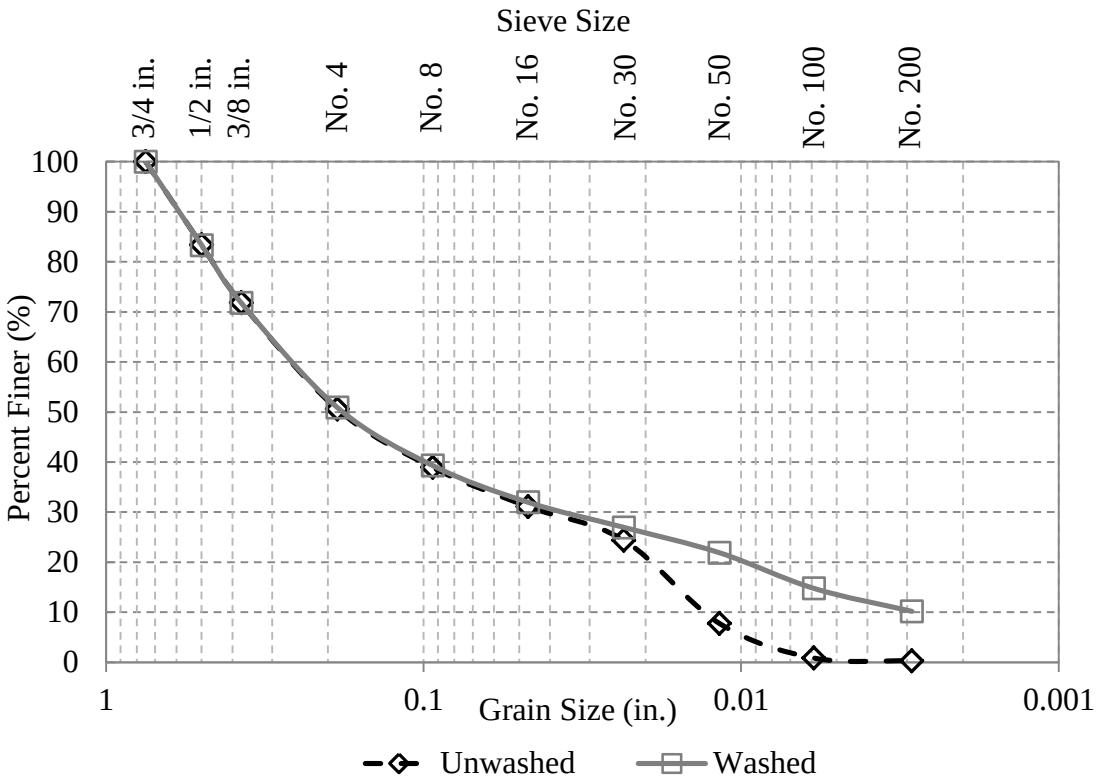

Figure A-6: Particle-size distribution for Vernal material.

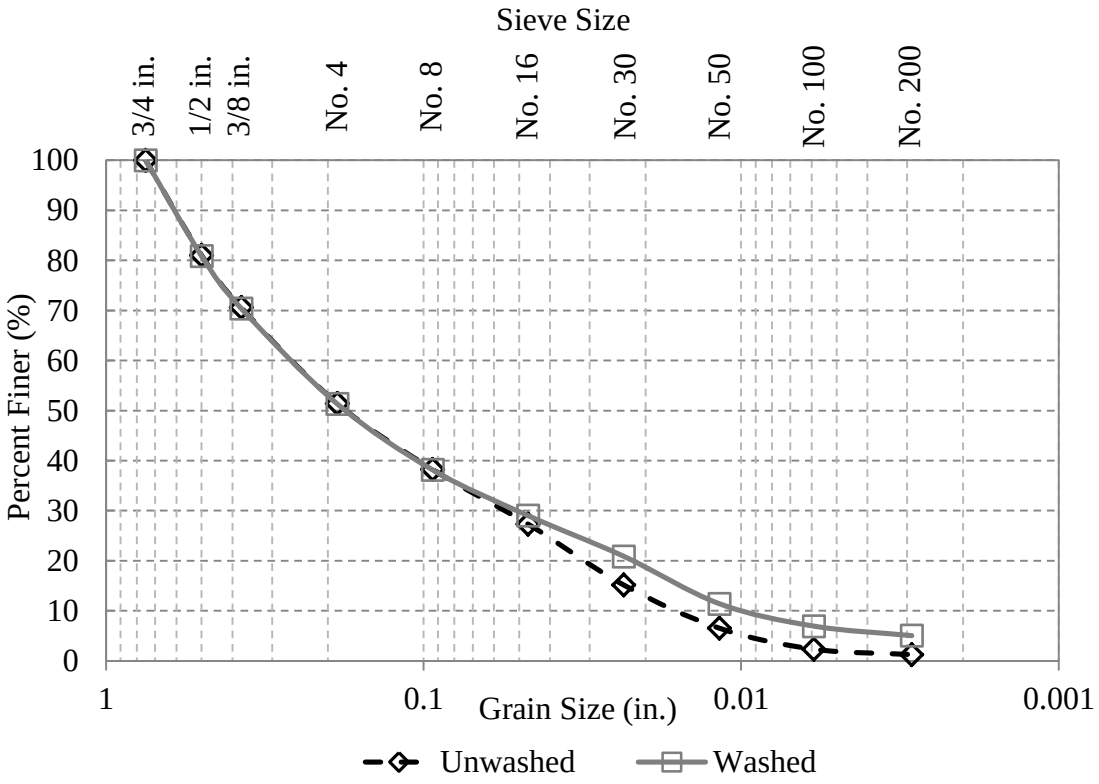

Figure A-7: Particle-size distribution for Elsinore material.

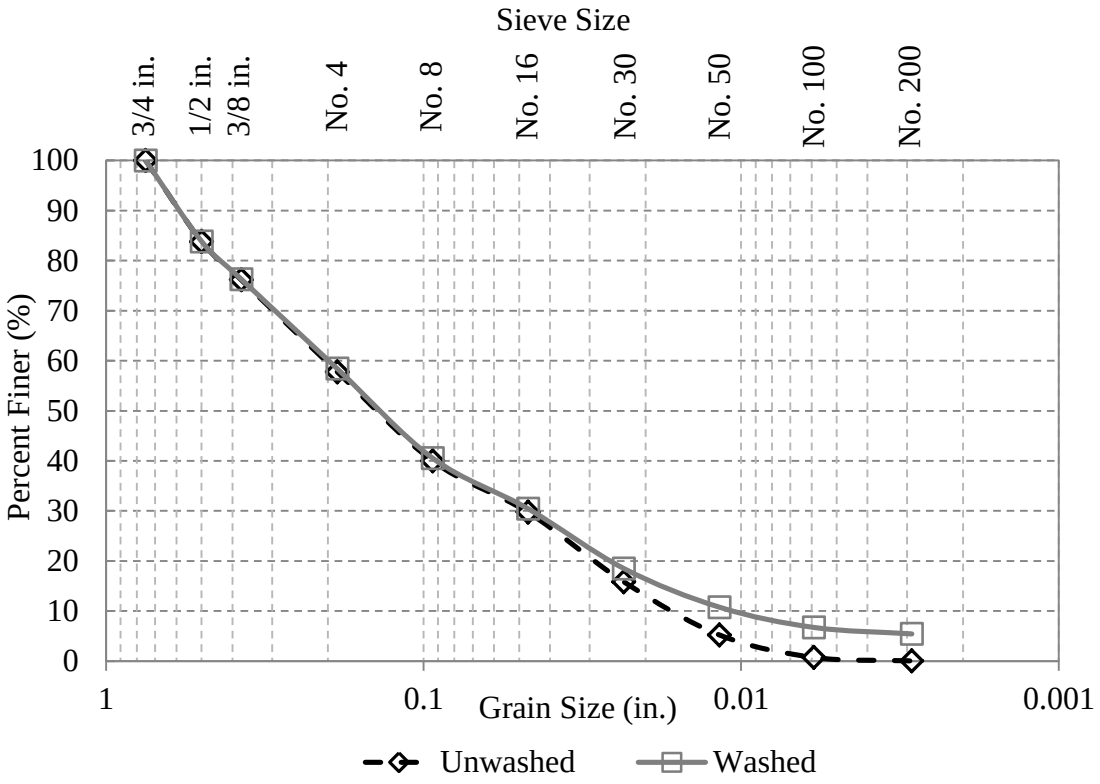

Figure A-8: Particle-size distribution for Nielson material.

APPENDIX B MOISTURE-DENSITY CURVES

Table B-1: Results of Moisture-Density Testing for McGuire Material

Moisture Content (%)	Dry Density (pcf)
4.6	136.7
5.2	137.7
5.6	139.2
6.0	139.0

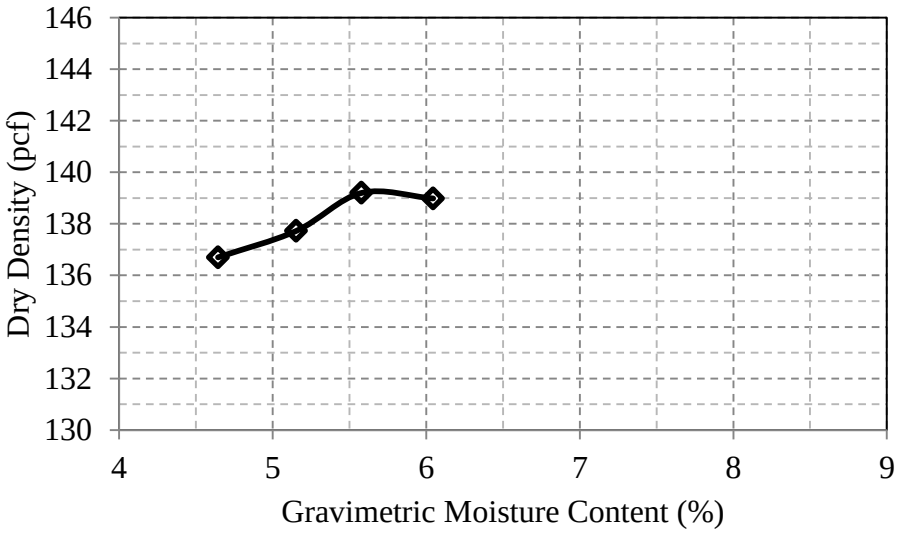

Figure B-1: Moisture-density curve for McGuire material.

Table B-2: Results of Moisture-Density Testing for Trenton Material

Moisture Content (%)	Dry Density (pcf)
4.4	139.7
5.4	142.1
6.0	141.8
6.4	141.0
7.2	138.4

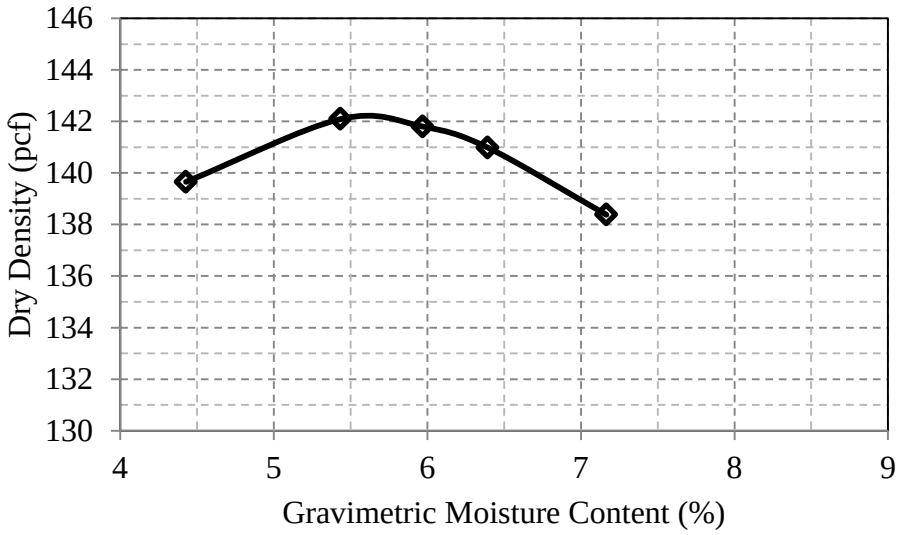

Figure B-2: Moisture-density curve for Trenton material.

Table B-3: Results of Moisture-Density Testing for Beck St. Material

Moisture Content (%)	Dry Density (pcf)
5.8	144.8
6.3	145.0
6.8	144.5

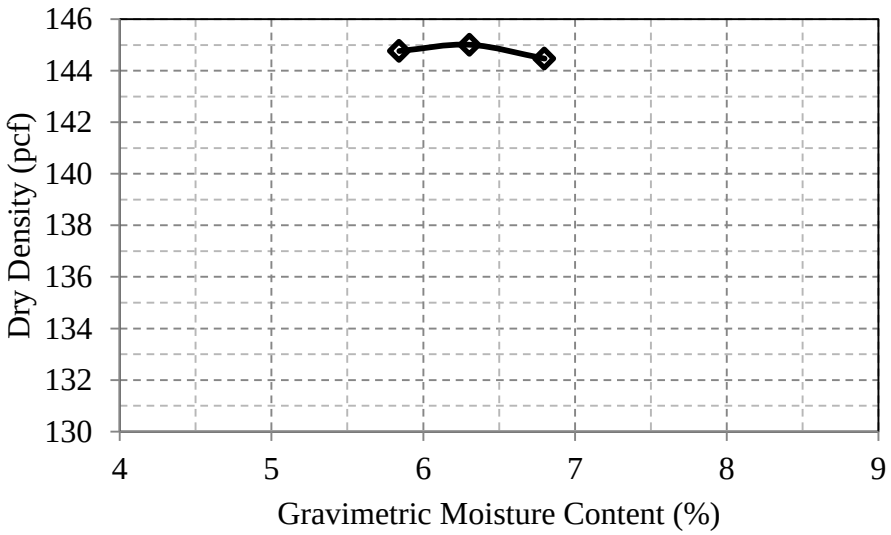

Figure B-3: Moisture-density curve for Beck St. material.

Table B-4: Results of Moisture-Density Testing for Parley's Canyon Material

Moisture Content (%)	Dry Density (pcf)
5.1	141.2
6.0	143.0
6.5	142.3
6.8	141.5
7.4	138.6

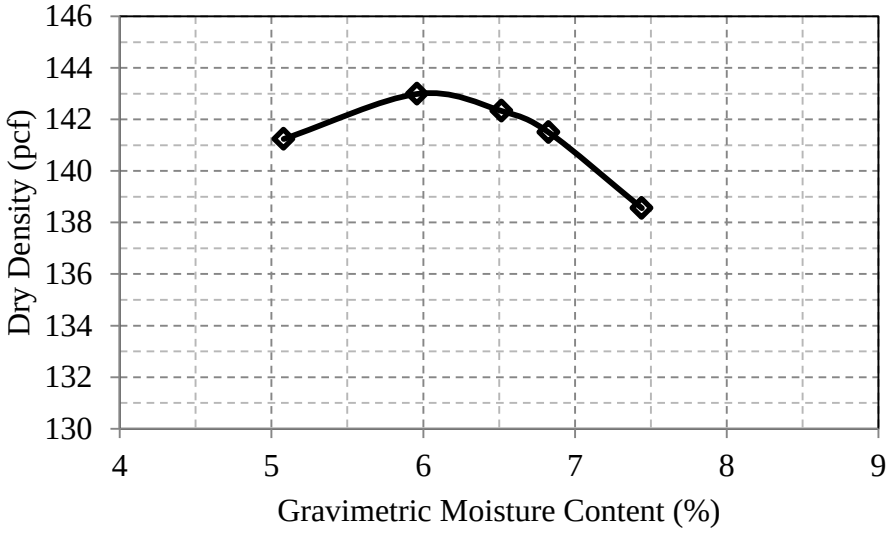

Figure B-4: Moisture-density curve for Parley's Canyon material.

Table B-5: Results of Moisture-Density Testing for Point of the Mountain Material

Moisture Content (%)	Dry Density (pcf)
5.9	137.2
6.2	137.4
6.6	137.4
7.2	137.0

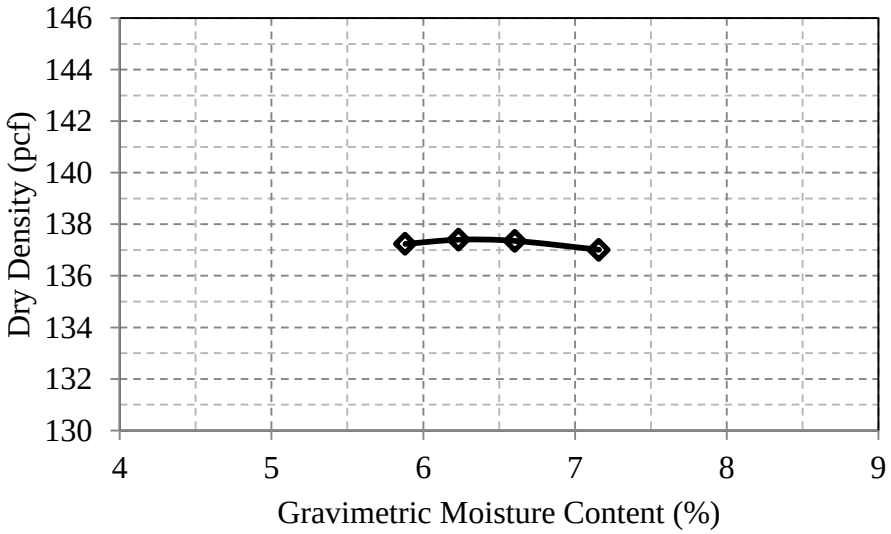

Figure B-5: Moisture-density curve for Point of the Mountain material.

Table B-6: Results of Moisture-Density Testing for Vernal Material

Moisture Content (%)	Dry Density (pcf)
5.4	139.5
6.7	140.3
7.4	138.9
8.3	136.7

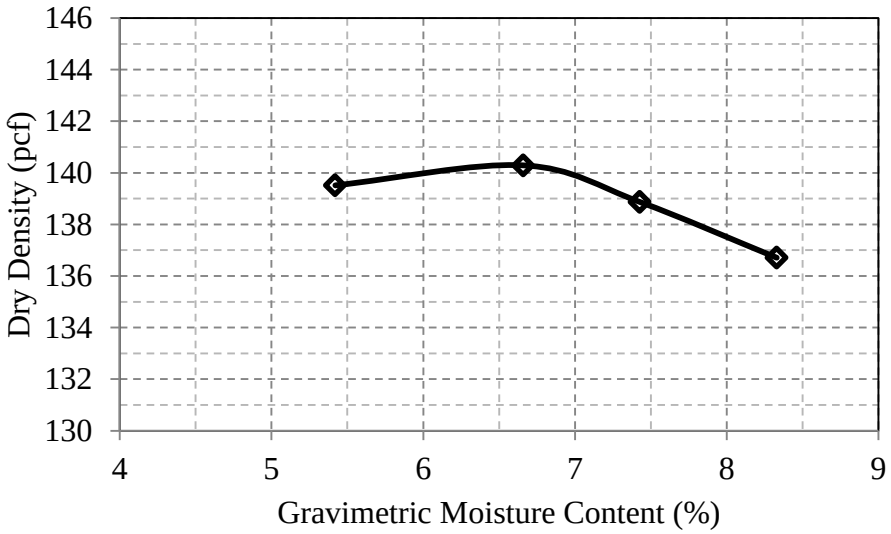

Figure B-6: Moisture-density curve for Vernal material.

Table B-7: Results of Moisture-Density Testing for Elsinore Material

Moisture Content (%)	Dry Density (pcf)
4.8	130.7
5.7	134.8
6.2	137.3
6.7	136.1
7.2	134.9

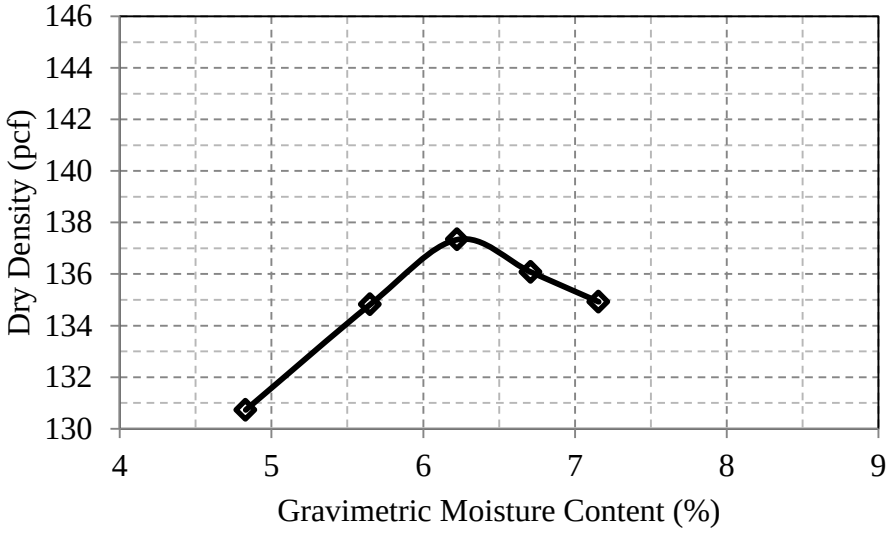

Figure B-7: Moisture-density curve for Elsinore material.

Table B-8: Results of Moisture-Density Testing for Nielson Material

Moisture Content (%)	Dry Density (pcf)
4.7	135.2
5.1	137.9
5.5	138.6
5.8	137.1
5.9	136.9

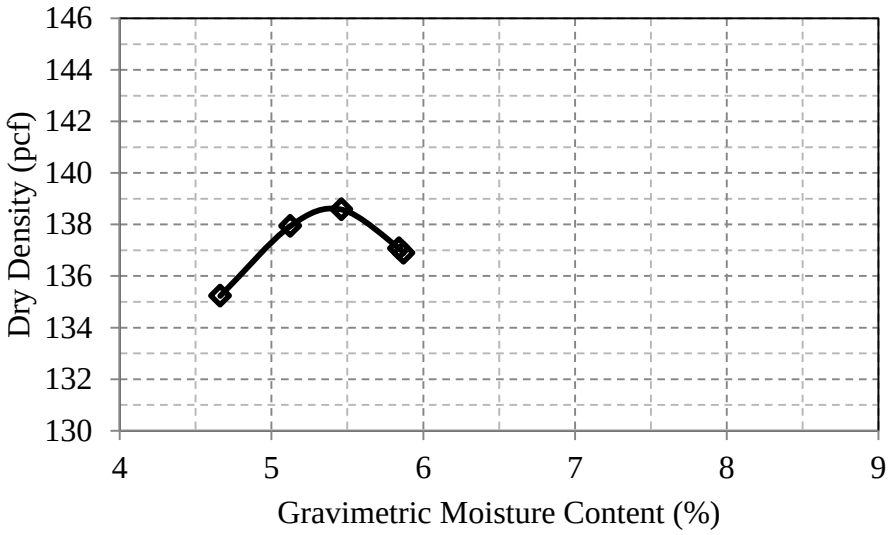

Figure B-8: Moisture-density curve for Nielson material.

APPENDIX C RESULTS OF CALIFORNIA BEARING RATIO TESTING

Table C-1: Results of California Bearing Ratio Testing by Specimen

UDOT Region	Material	Specimen	Dry Density (pcf)	CBR
1	McGuire	1	136.8	102
		2	136.7	86
	Trenton	1	137.7	64
		2	138.0	82
		3	137.1	33
2	Beck St.	1	142.5	50
		2	143.6	54
	Parley's Canyon	1	140.1	20
		2	140.0	39
		3	140.2	42
3	Point of the Mountain	1	138.0	111
		2	138.4	107
	Vernal	1	139.3	19
		2	138.8	17
4	Elsinore	1	136.4	62
		2	134.0	115
		3	133.5	103
	Nielson	1	136.8	87
		2	137.3	76

APPENDIX D RESULTS OF RESILIENT MODULUS TESTING

Table D-1: Results of Resilient Modulus Testing by Specimen

UDOT Region	Material	Specimen	Dry Density (pcf)	Resilient Modulus (ksi)	K_1	K_2
1	McGuire	1	136.3	21.8	1159	0.747
		2	138.2	22.0	990	0.790
		3	139.3	16.8	1785	0.582
	Trenton	1	138.1	18.2	2097	0.556
		2	131.1	25.1	1591	0.705
		3	131.5	27.4	1633	0.715
		4	131.4	24.2	1967	0.642
		5	142.1	17.1	2588	0.488
2	Beck St.	1	145.7	17.7	2827	0.476
		2	153.6	22.6	3079	0.516
		3	154.5	20.1	2773	0.515
		4	148.2	24.0	2508	0.580
		5	145.3	20.0	3264	0.471
	Parley's Canyon	1	140.6	21.1	2566	0.544
		2	141.9	20.5	2109	0.588
		3	141.2	22.3	1921	0.631
3	Point of the Mountain	1	138.3	15.2	2132	0.509
		2	139.1	16.4	982	0.722
		3	140.1	16.3	1611	0.596
		4	138.9	16.0	1845	0.556
	Vernal	1	138.2	19.1	2635	0.508
		2	139.7	20.6	1780	0.633
		3	138.7	21.8	2512	0.557
4	Elsinore	1	133.4	22.5	1703	0.657
		2	137.0	16.6	1044	0.715
		3	142.4	14.4	1272	0.628
		4	136.0	21.1	1174	0.732
	Nielson	1	137.4	34.9	2904	0.627
		2	143.6	17.8	1465	0.645
		3	140.7	18.4	1744	0.609
		4	137.0	31.2	2705	0.621

Table D-2: Results of Resilient Modulus Test 1 for McGuire Material

Sequence	Stress Invariant (psi)	Resilient Modulus (ksi)
1	11.6865	12.1
2	14.4095	7.4
3	17.0950	5.7
4	19.5102	16.8
5	23.9889	10.2
6	28.5134	7.6
7	38.9666	26.8
8	47.9314	15.8
9	56.9436	11.4
10	53.9795	44.4
11	58.4751	33.1
12	71.9463	20.1
13	73.4704	49.8
14	77.9688	41.3
15	95.9595	24.5

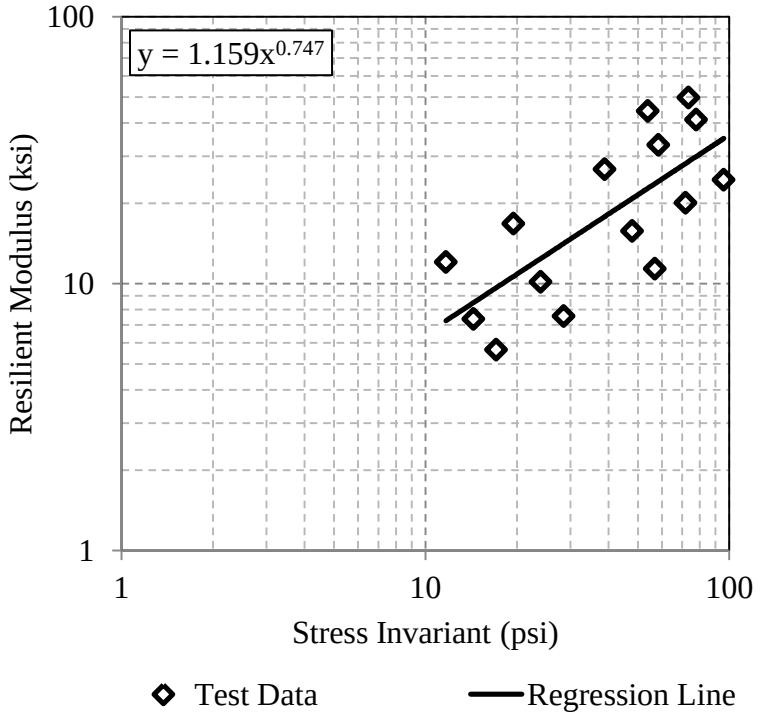

Figure D-1: Analysis of resilient modulus test 1 for McGuire material.

Table D-3: Results of Resilient Modulus Test 2 for McGuire Material

Sequence	Stress Invariant (psi)	Resilient Modulus (ksi)
1	11.6868	11.8
2	14.4107	7.1
3	17.1011	5.6
4	19.4939	15.8
5	23.9869	9.7
6	28.4989	7.5
7	38.9581	25.5
8	47.9539	15.8
9	56.9550	11.6
10	53.9739	45.3
11	58.4813	33.7
12	71.9646	20.9
13	73.4928	51.3
14	77.9748	42.5
15	95.9607	26.0

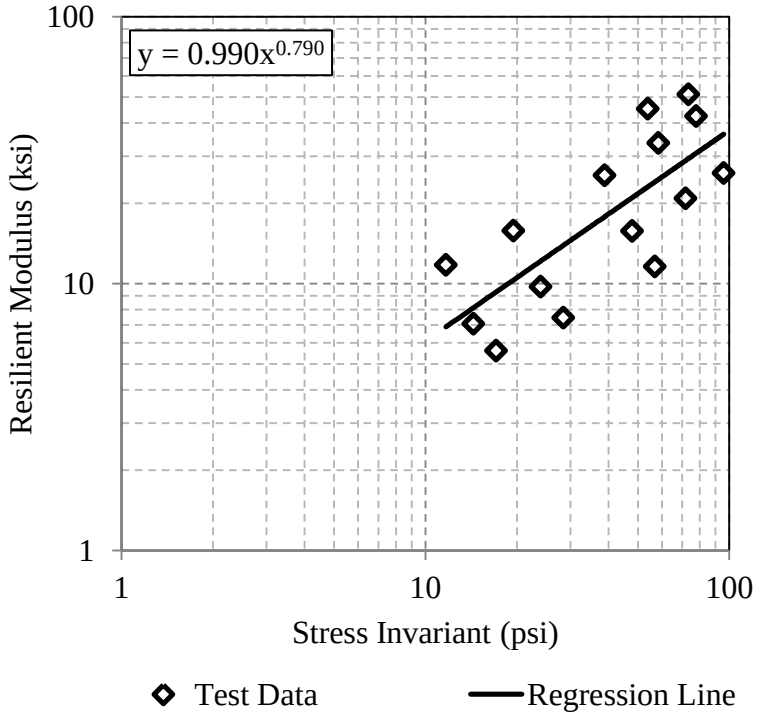

Figure D-2: Analysis of resilient modulus test 2 for McGuire material.

Table D-4: Results of Resilient Modulus Test 3 for McGuire Material

Sequence	Stress Invariant (psi)	Resilient Modulus (ksi)
1	11.6917	12.9
2	14.4119	7.8
3	17.0963	5.8
4	19.5040	14.0
5	23.9932	9.4
6	28.4751	7.3
7	38.9615	18.8
8	47.9586	13.7
9	56.9399	10.8
10	53.9725	27.2
11	58.4730	23.2
12	71.9497	17.6
13	73.4808	32.6
14	77.9747	29.9
15	95.9662	21.8

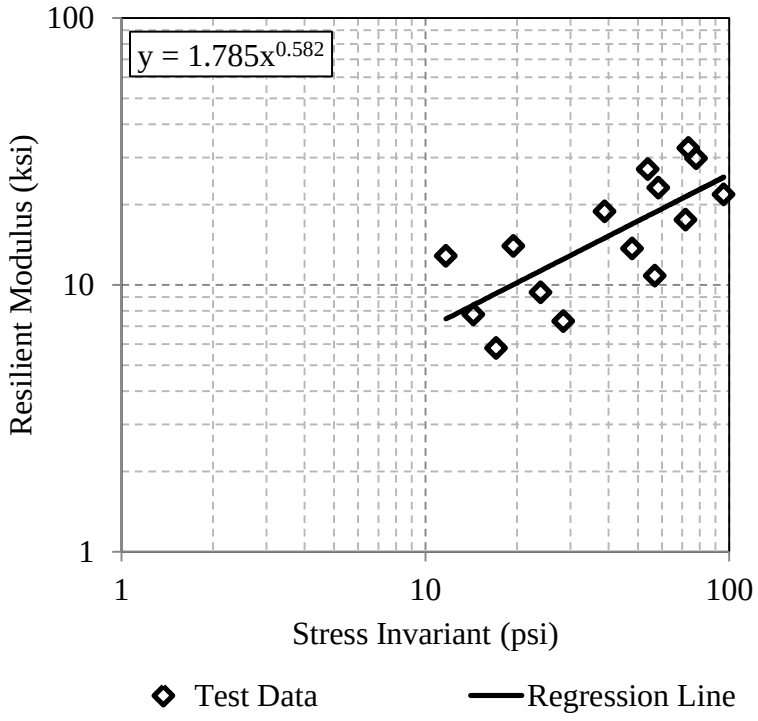

Figure D-3: Analysis of resilient modulus test 3 for McGuire material.

Table D-5: Results of Resilient Modulus Test 1 for Trenton Material

Sequence	Stress Invariant (psi)	Resilient Modulus (ksi)
1	11.6958	13.3
2	14.3963	8.3
3	17.1023	6.4
4	19.4965	15.5
5	23.9993	10.5
6	28.5010	7.9
7	38.9587	21.6
8	47.9510	14.1
9	56.9396	10.9
10	53.9573	34.3
11	58.4896	25.0
12	71.9589	17.4
13	73.4932	37.0
14	77.9775	30.5
15	95.9581	20.6

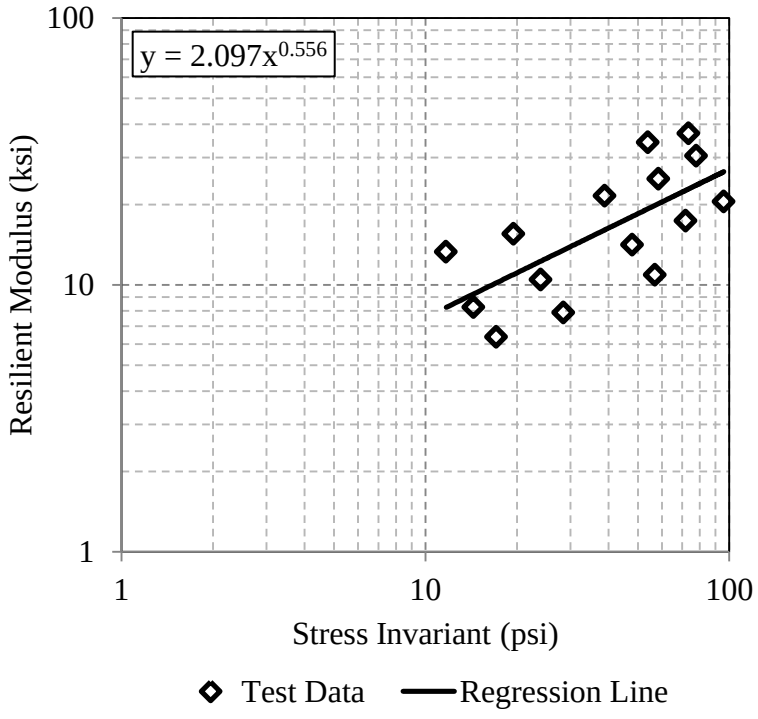

Figure D-4: Analysis of resilient modulus test 1 for Trenton material.

Table D-6: Results of Resilient Modulus Test 2 for Trenton Material

Sequence	Stress Invariant (psi)	Resilient Modulus (ksi)
1	11.6919	15.2
2	14.4031	8.9
3	17.0923	7.0
4	19.4894	19.6
5	23.9867	12.4
6	28.4931	9.4
7	38.9550	30.3
8	47.9590	19.0
9	56.9211	13.8
10	53.9705	48.8
11	58.4865	37.7
12	71.9579	23.7
13	73.4918	55.2
14	77.9851	46.9
15	95.9584	28.7

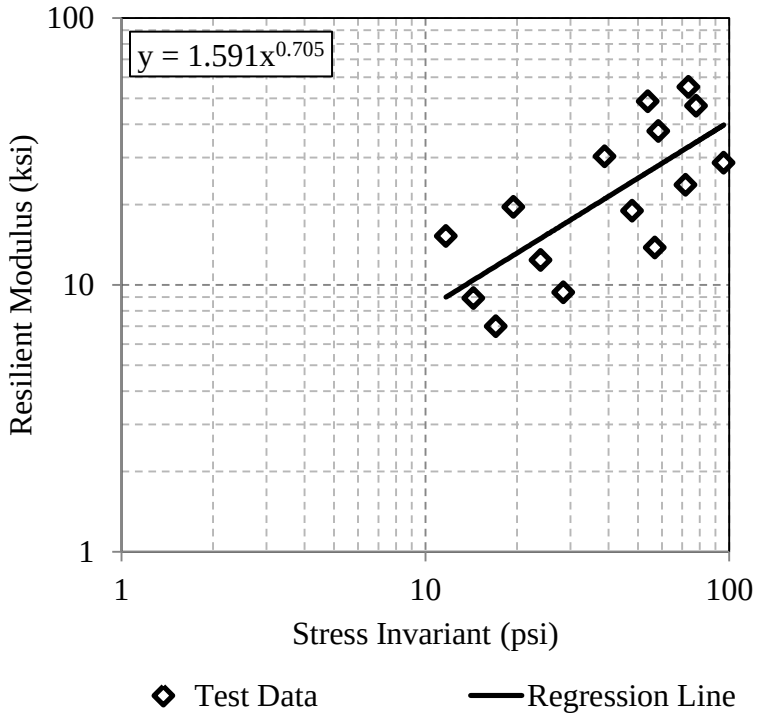

Figure D-5: Analysis of resilient modulus test 2 for Trenton material.

Table D-7: Results of Resilient Modulus Test 3 for Trenton Material

Sequence	Stress Invariant (psi)	Resilient Modulus (ksi)
1	11.6901	16.6
2	14.3996	9.3
3	17.1011	7.2
4	19.5000	21.3
5	23.9756	12.8
6	28.5027	9.4
7	38.9489	34.0
8	47.9664	19.2
9	56.9580	13.6
10	53.9590	58.3
11	58.4556	41.2
12	71.9392	24.2
13	73.4900	63.5
14	77.9711	51.3
15	95.9362	29.3

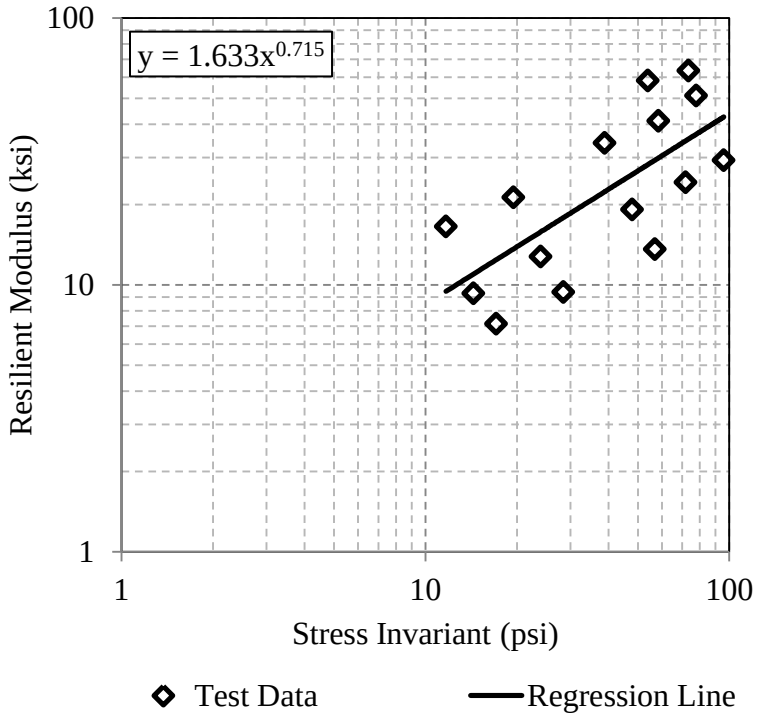

Figure D-6: Analysis of resilient modulus test 3 for Trenton material.

Table D-8: Results of Resilient Modulus Test 4 for Trenton Material

Sequence	Stress Invariant (psi)	Resilient Modulus (ksi)
1	11.6933	16.6
2	14.3916	9.1
3	17.1002	7.0
4	19.5062	21.1
5	23.9965	12.5
6	28.5099	9.2
7	38.9595	30.3
8	47.9453	18.6
9	56.9321	13.2
10	53.9551	46.1
11	58.4597	35.8
12	71.9356	23.1
13	73.4743	49.8
14	77.9782	43.0
15	95.9622	27.9

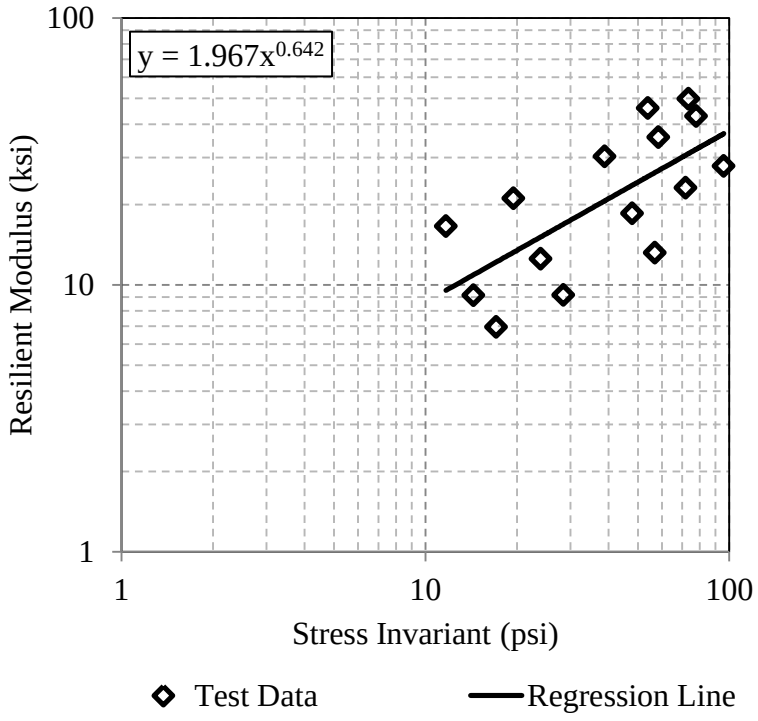

Figure D-7: Analysis of resilient modulus test 4 for Trenton material.

Table D-9: Results of Resilient Modulus Test 5 for Trenton Material

Sequence	Stress Invariant (psi)	Resilient Modulus (ksi)
1	11.6787	13.4
2	14.3915	8.4
3	17.1085	6.4
4	19.4813	16.3
5	23.9850	10.5
6	28.5038	7.9
7	38.9466	21.4
8	47.9368	14.5
9	56.9334	10.5
10	53.9846	28.5
11	58.4973	23.5
12	71.9514	16.8
13	73.4647	30.8
14	77.9531	28.4
15	95.9930	18.7

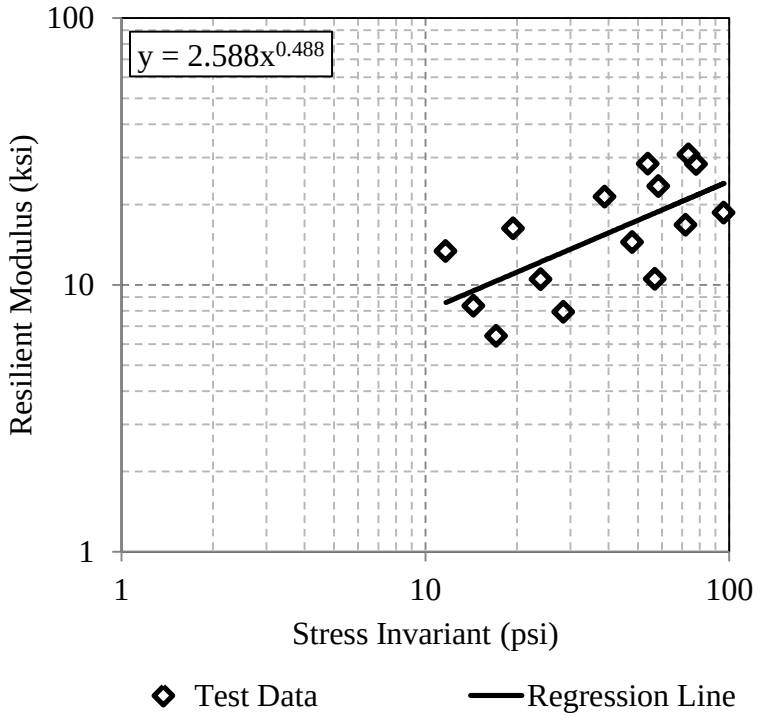

Figure D-8: Analysis of resilient modulus test 5 for Trenton material.

Table D-10: Results of Resilient Modulus Test 1 for Beck St. Material

Sequence	Stress Invariant (psi)	Resilient Modulus (ksi)
1	11.6883	14.6
2	14.4179	9.1
3	17.1060	7.0
4	19.4887	16.2
5	23.9893	11.0
6	28.5079	8.6
7	38.9551	21.2
8	47.9572	14.4
9	56.9537	11.0
10	53.9438	29.3
11	58.4657	23.4
12	71.9486	17.1
13	73.4679	32.5
14	77.9677	29.2
15	95.9643	21.1

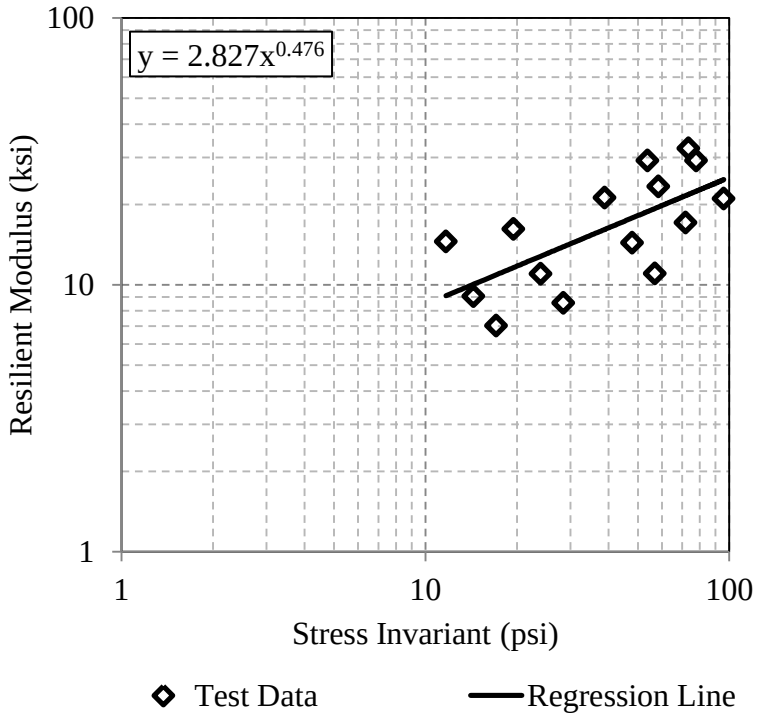

Figure D-9: Analysis of resilient modulus test 1 for Beck St. material.

Table D-11: Results of Resilient Modulus Test 2 for Beck St. Material

Sequence	Stress Invariant (psi)	Resilient Modulus (ksi)
1	11.6883	17.7
2	14.4000	11.2
3	17.1205	8.7
4	19.5067	19.6
5	24.0155	13.4
6	28.5184	10.4
7	38.9649	26.0
8	47.9669	18.0
9	56.9527	14.4
10	53.9702	38.1
11	58.4836	30.5
12	71.9930	22.1
13	73.4712	43.3
14	77.9925	38.3
15	95.9768	27.1

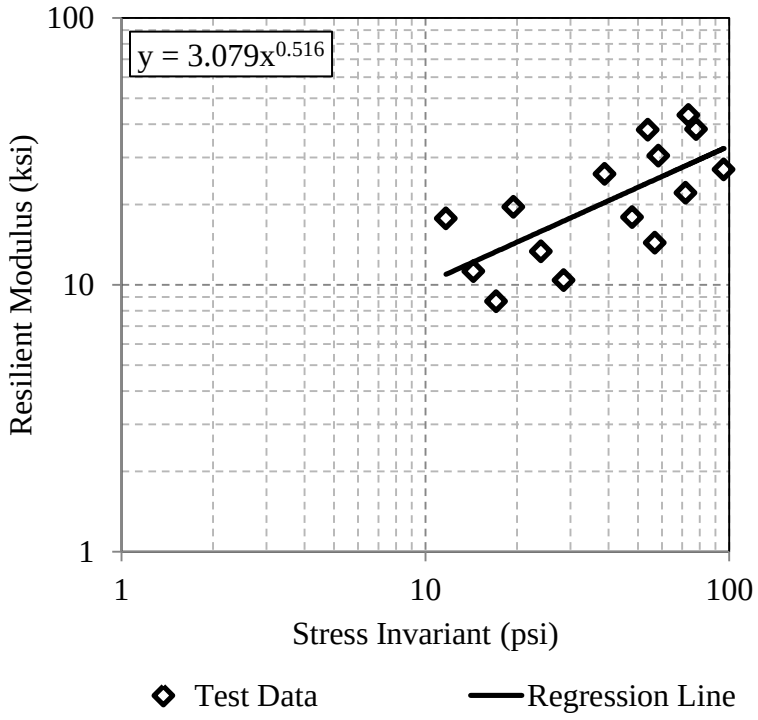

Figure D-10: Analysis of resilient modulus test 2 for Beck St. material.

Table D-12: Results of Resilient Modulus Test 3 for Beck St. Material

Sequence	Stress Invariant (psi)	Resilient Modulus (ksi)
1	11.6909	16.0
2	14.3991	9.9
3	17.1042	7.7
4	19.4931	17.5
5	23.9833	12.1
6	28.4864	9.5
7	38.9650	23.3
8	47.9841	16.4
9	56.9620	13.2
10	53.9692	33.3
11	58.4839	28.2
12	71.9652	20.9
13	73.4863	36.1
14	77.9915	33.1
15	95.9649	24.2

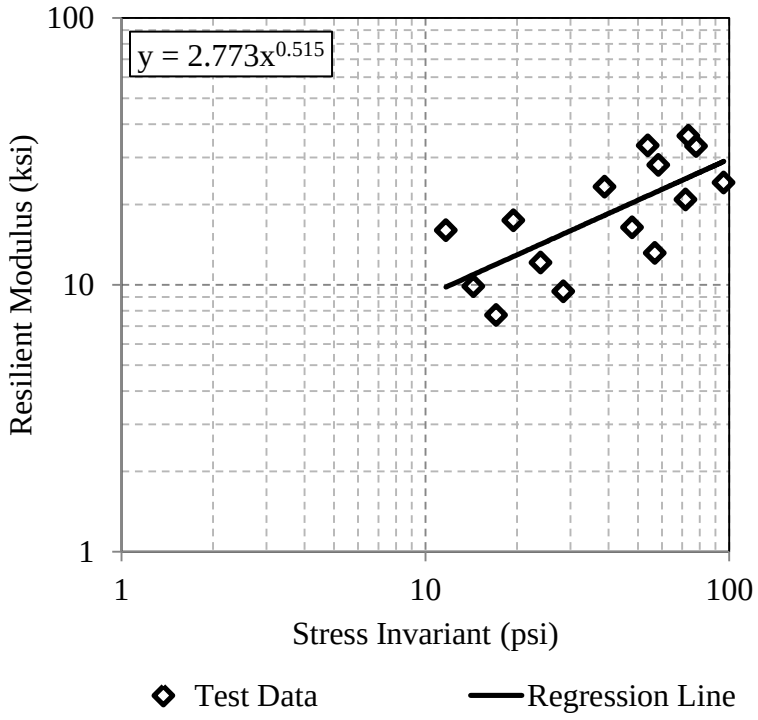

Figure D-11: Analysis of resilient modulus test 3 for Beck St. material.

Table D-13: Results of Resilient Modulus Test 4 for Beck St. Material

Sequence	Stress Invariant (psi)	Resilient Modulus (ksi)
1	11.6993	17.7
2	14.4159	10.8
3	17.1105	8.2
4	19.5012	19.2
5	23.9890	13.1
6	28.5088	10.2
7	38.9463	26.9
8	47.9437	17.9
9	56.9454	14.1
10	53.9664	44.5
11	58.4828	33.5
12	71.9289	22.1
13	73.4977	51.6
14	77.9698	43.3
15	95.9611	27.3

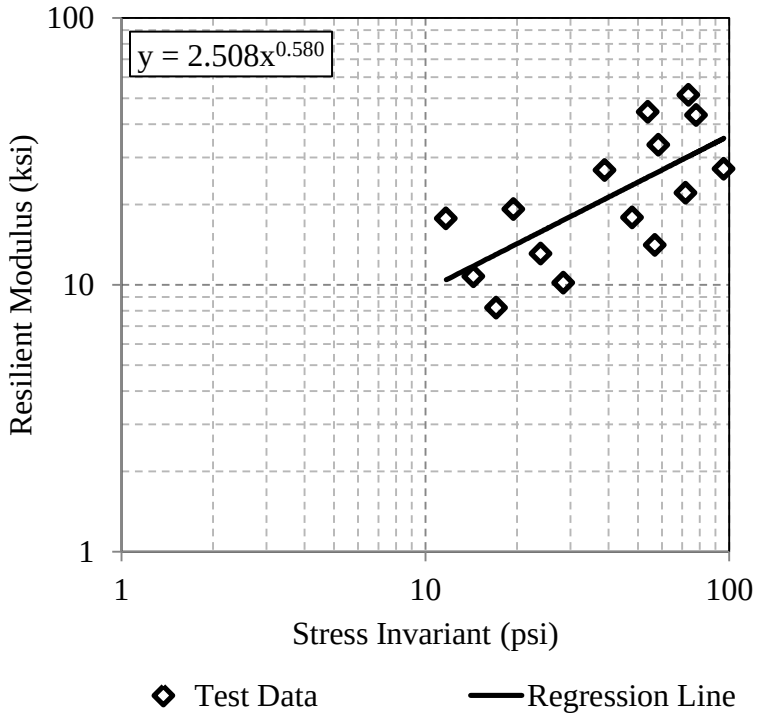

Figure D-12: Analysis of resilient modulus test 4 for Beck St. material.

Table D-14: Results of Resilient Modulus Test 5 for Beck St. Material

Sequence	Stress Invariant (psi)	Resilient Modulus (ksi)
1	11.6899	16.6
2	14.3972	10.3
3	17.1041	7.9
4	19.4879	18.4
5	23.9880	12.4
6	28.5009	9.6
7	38.9518	24.2
8	47.9643	16.7
9	56.9296	13.2
10	53.9686	33.0
11	58.5012	27.8
12	71.9691	20.2
13	73.4894	35.3
14	78.0074	31.7
15	95.9538	22.8

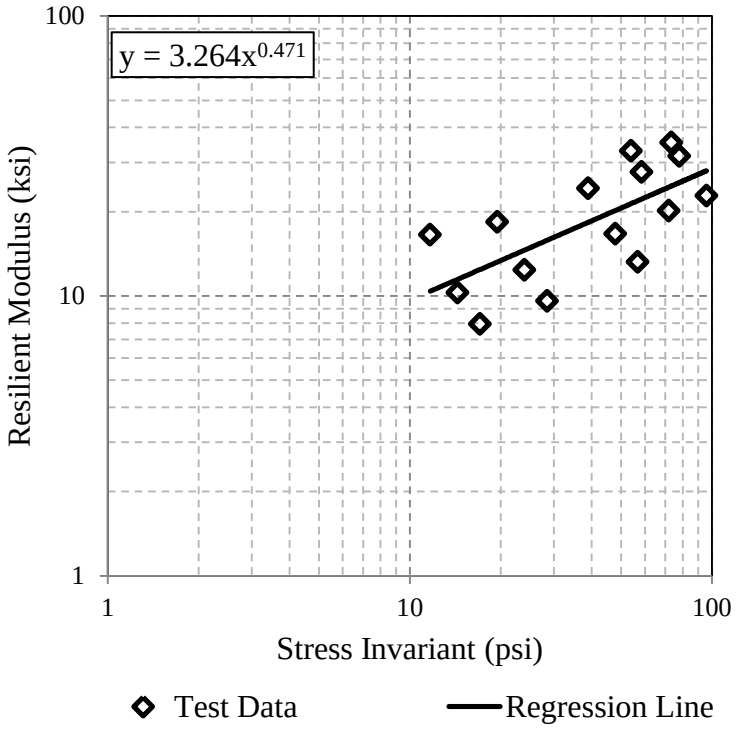

Figure D-13: Analysis of resilient modulus test 5 Beck St. material.

Table D-15: Results of Resilient Modulus Test 1 for Parley's Canyon Material

Sequence	Stress Invariant (psi)	Resilient Modulus (ksi)
1	11.6941	14.9
2	14.3983	9.6
3	17.1026	7.7
4	19.4952	18.9
5	24.0007	12.7
6	28.5059	9.5
7	38.9669	25.7
8	47.9502	16.7
9	56.9522	12.6
10	53.9773	36.5
11	58.4523	29.5
12	71.9603	20.6
13	73.4952	40.8
14	77.9955	36.4
15	95.9813	23.7

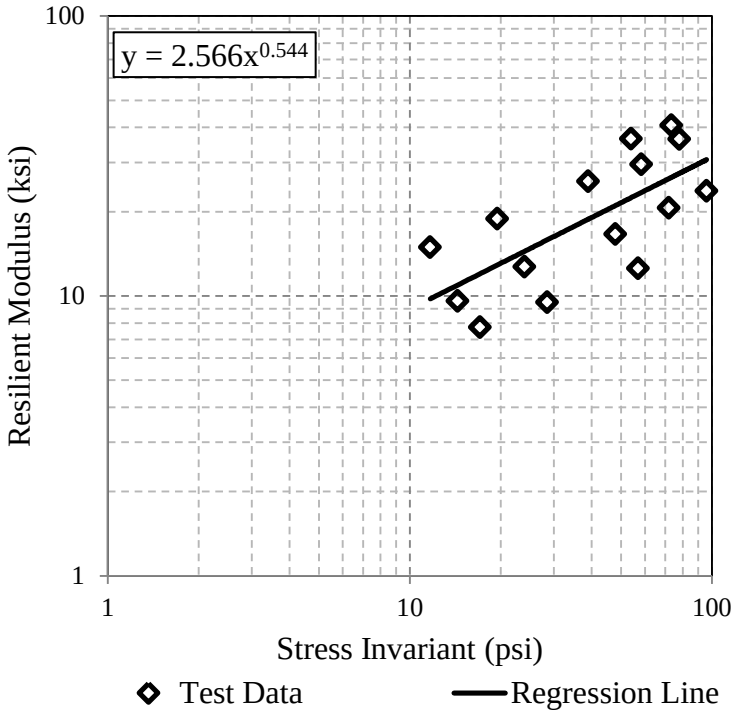

Figure D-14: Analysis of resilient modulus test 1 for Parley's Canyon material.

Table D-16: Results of Resilient Modulus Test 2 for Parley's Canyon Material

Sequence	Stress Invariant (psi)	Resilient Modulus (ksi)
1	11.6832	14.6
2	14.4048	8.9
3	17.0977	6.9
4	19.4838	17.6
5	23.9812	11.8
6	28.4889	9.0
7	38.9588	24.3
8	47.9571	16.3
9	56.9399	12.9
10	53.9656	35.6
11	58.4669	29.2
12	71.9575	21.0
13	73.4742	39.7
14	77.9800	36.2
15	96.0057	24.1

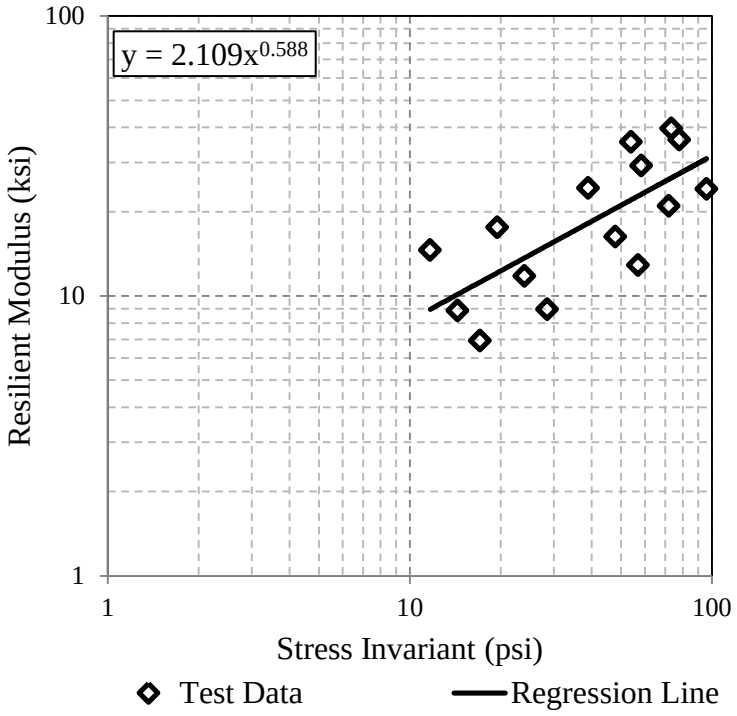

Figure D-15: Analysis of resilient modulus test 2 for Parley's Canyon material.

Table D-17: Results of Resilient Modulus Test 3 for Parley's Canyon Material

Sequence	Stress Invariant (psi)	Resilient Modulus (ksi)
1	11.6904	13.6
2	14.4057	9.1
3	17.0955	7.3
4	19.4872	19.1
5	23.9891	12.5
6	28.5014	9.4
7	38.9651	26.4
8	47.9484	17.3
9	56.9436	13.1
10	53.9821	41.7
11	58.4697	31.8
12	71.9497	21.4
13	73.4984	46.8
14	77.9760	39.7
15	95.9926	25.4

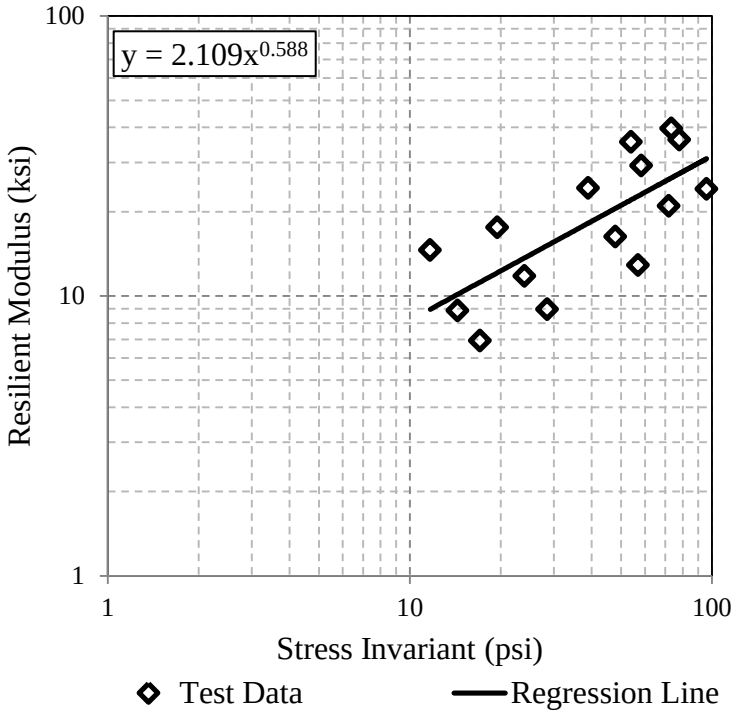

Figure D-16: Analysis of resilient modulus test 3 for Parley's Canyon material.

Table D-18: Results of Resilient Modulus Test 1 for Point of the Mountain Material

Sequence	Stress Invariant (psi)	Resilient Modulus (ksi)
1	11.6932	11.9
2	14.4097	7.6
3	17.0986	5.9
4	19.4872	13.3
5	23.9871	9.1
6	28.4847	7.1
7	38.9454	17.7
8	47.9502	12.2
9	56.9480	9.5
10	53.9658	26.2
11	58.4900	20.8
12	71.9743	14.8
13	73.4841	29.1
14	77.9797	25.5
15	95.9929	17.8

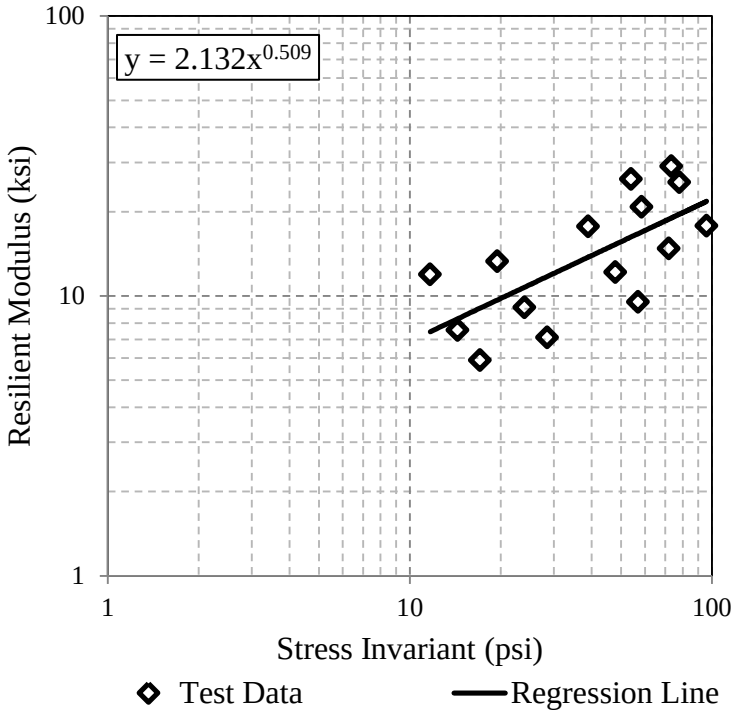

Figure D-17: Analysis of resilient modulus test 1 for Point of the Mountain material.

Table D-19: Results of Resilient Modulus Test 2 for Point of the Mountain Material

Sequence	Stress Invariant (psi)	Resilient Modulus (ksi)
1	11.6860	9.6
2	14.4080	6.2
3	17.1122	4.9
4	19.4919	11.7
5	23.9912	7.8
6	28.4950	6.2
7	38.9649	18.6
8	47.9615	11.9
9	56.9301	9.4
10	53.9791	31.8
11	58.4946	24.0
12	71.9628	15.8
13	73.4900	36.6
14	77.9629	31.4
15	95.9499	20.3

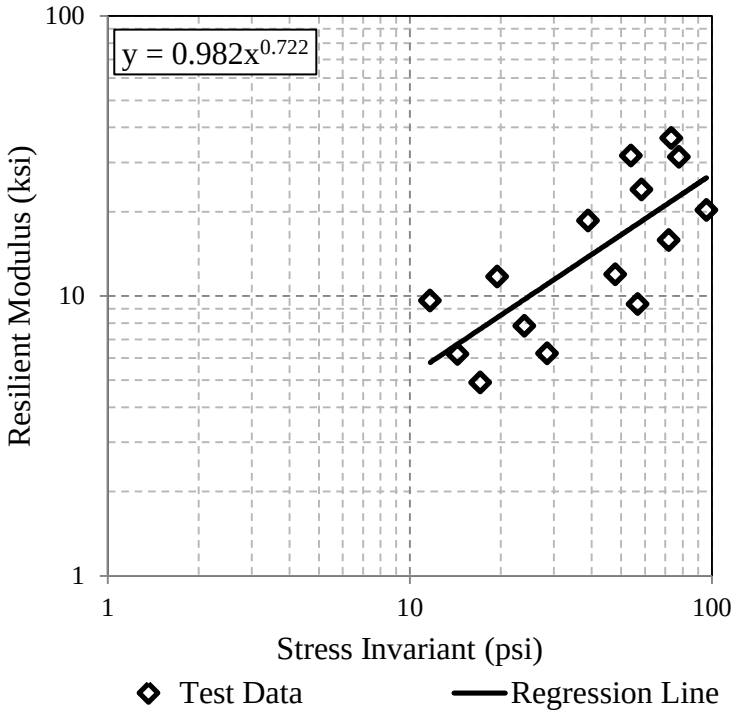

Figure D-18: Analysis of resilient modulus test 2 for Point of the Mountain material.

Table D-20: Results of Resilient Modulus Test 3 for Point of the Mountain Material

Sequence	Stress Invariant (psi)	Resilient Modulus (ksi)
1	11.6904	11.1
2	14.4125	7.2
3	17.0985	5.7
4	19.4867	13.0
5	24.0073	9.0
6	28.4947	7.2
7	38.9576	18.6
8	47.9627	12.4
9	56.9353	9.9
10	53.9632	29.4
11	58.4712	22.6
12	71.9555	15.4
13	73.4966	34.4
14	77.9754	29.2
15	95.9669	19.0

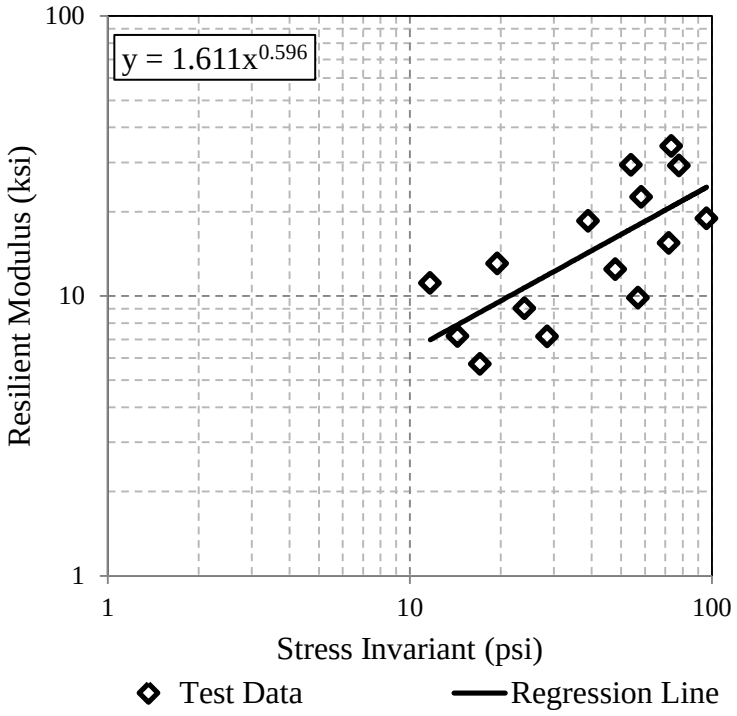

Figure D-19: Analysis of resilient modulus test 3 for Point of the Mountain material.

Table D-21: Results of Resilient Modulus Test 4 for Point of the Mountain Material

Sequence	Stress Invariant (psi)	Resilient Modulus (ksi)
1	11.6991	12.0
2	14.4175	7.5
3	17.1094	5.8
4	19.4905	13.1
5	23.9902	9.0
6	28.5038	7.0
7	38.9806	18.1
8	47.9646	12.0
9	56.9559	9.5
10	53.9642	29.0
11	58.4849	22.0
12	71.9604	14.9
13	73.4809	33.6
14	77.9755	28.4
15	95.9884	18.3

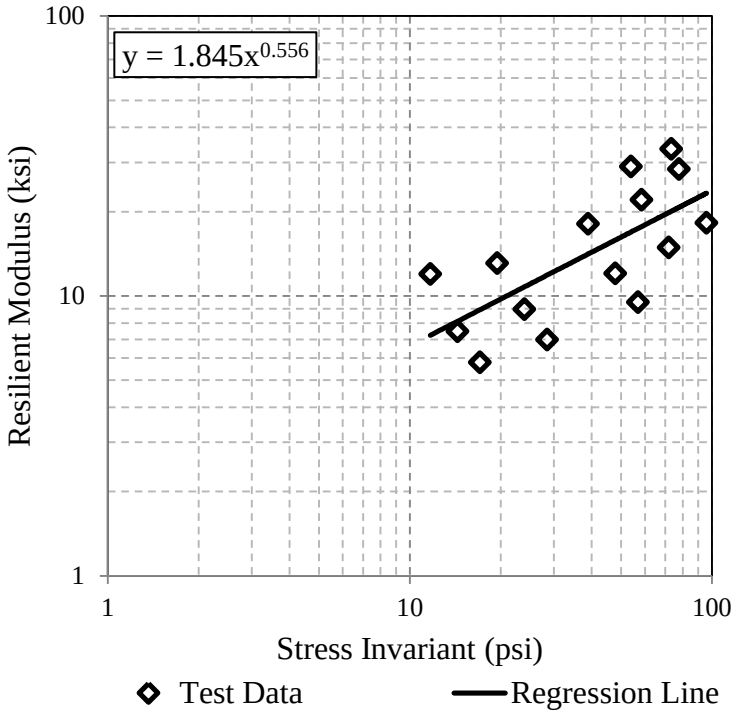

Figure D-20: Analysis of resilient modulus test 4 for Point of the Mountain material.

Table D-22: Results of Resilient Modulus for Test 1 Vernal Material

Sequence	Stress Invariant (psi)	Resilient Modulus (ksi)
1	11.7037	14.0
2	14.4009	9.1
3	17.1146	7.1
4	19.4888	16.8
5	23.9889	11.6
6	28.5026	8.6
7	38.9698	21.8
8	47.9600	14.6
9	56.9513	12.0
10	53.9740	27.6
11	58.4777	45.2
12	71.9806	17.1
13	73.4933	32.1
14	77.9884	30.0
15	95.9978	19.1

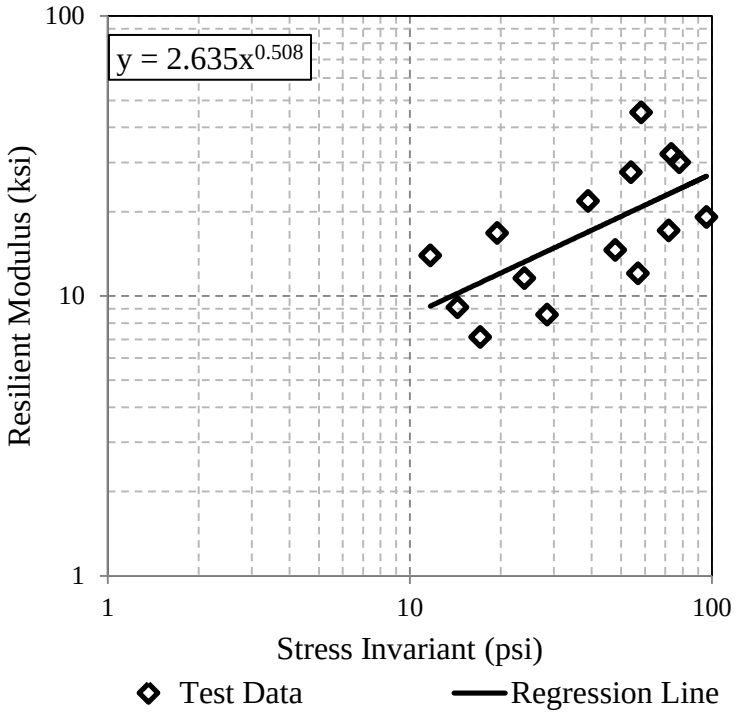

Figure D-21: Analysis of resilient modulus test 1 for Vernal material.

Table D-23: Results of Resilient Modulus Test 2 for Vernal Material

Sequence	Stress Invariant (psi)	Resilient Modulus (ksi)
1	11.7020	13.7
2	14.4208	8.7
3	17.1181	6.9
4	19.4978	16.2
5	23.9909	11.4
6	28.5032	8.8
7	38.9636	23.7
8	47.9500	16.3
9	56.9386	12.6
10	53.9770	35.7
11	58.4747	29.2
12	71.9619	21.0
13	73.5103	42.2
14	77.9709	37.8
15	95.9520	25.3

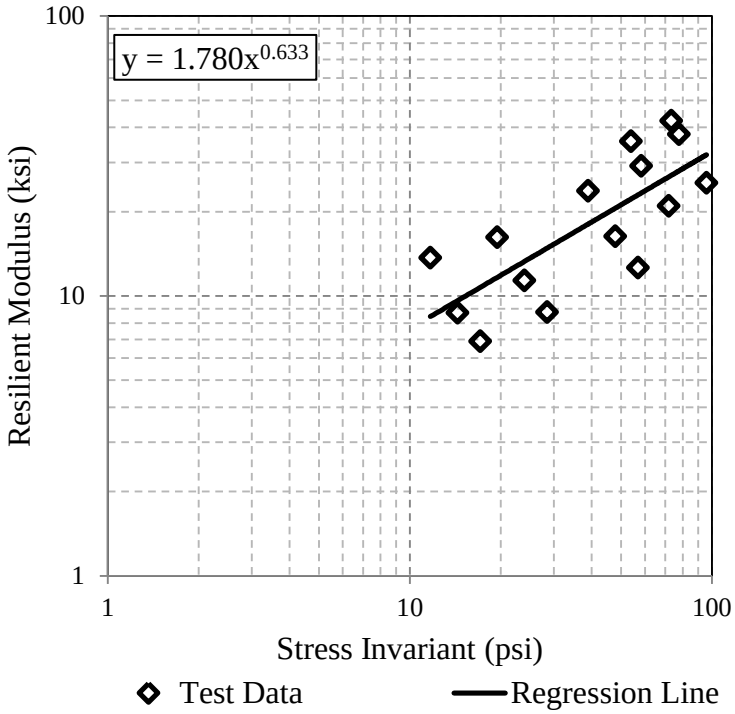

Figure D-22: Analysis of resilient modulus test 2 for Vernal material.

Table D-24: Results of Resilient Modulus Test 3 for Vernal Material

Sequence	Stress Invariant (psi)	Resilient Modulus (ksi)
1	11.7036	16.4
2	14.4199	10.0
3	17.0954	7.7
4	19.5045	18.6
5	24.0091	12.6
6	28.5062	9.4
7	38.9433	25.8
8	47.9500	16.9
9	56.9373	12.9
10	53.9670	37.1
11	58.4949	30.1
12	71.9448	21.4
13	73.4895	43.4
14	77.9664	38.7
15	95.9422	25.7

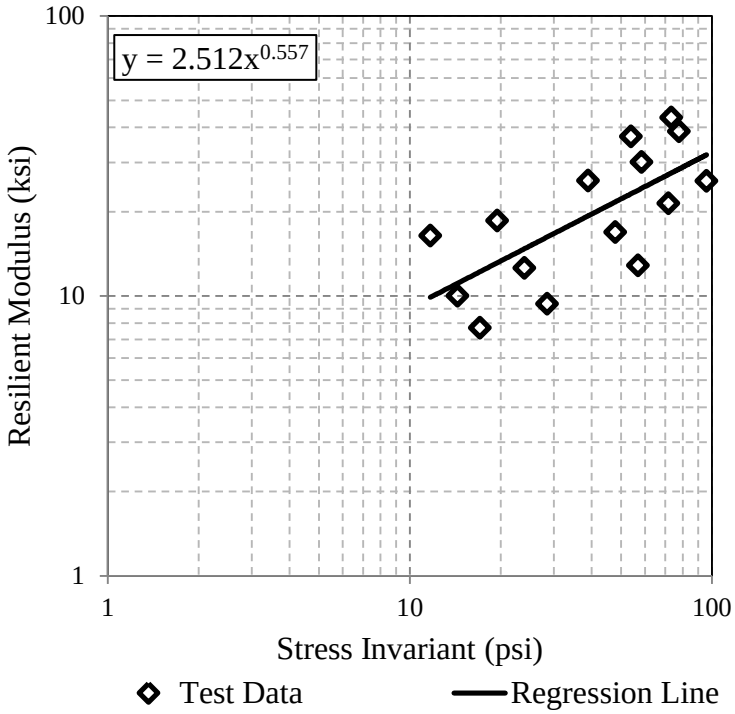

Figure D-23: Analysis of resilient modulus test 3 for Vernal material.

Table D-25: Results of Resilient Modulus Test 1 for Elsinore Material

Sequence	Stress Invariant (psi)	Resilient Modulus (ksi)
1	11.6879	14.9
2	14.4155	8.4
3	17.0876	6.4
4	19.5095	18.6
5	23.9941	11.1
6	28.5035	8.3
7	38.9560	28.0
8	47.9558	16.6
9	56.9640	11.8
10	53.9608	44.1
11	58.4692	33.2
12	71.9632	20.4
13	73.4847	49.5
14	77.9769	41.1
15	95.9762	24.6

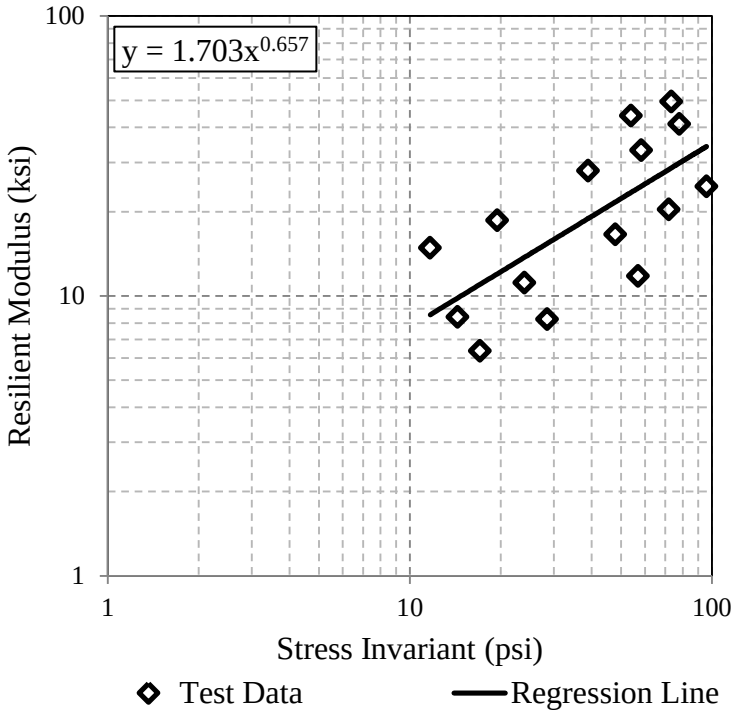

Figure D-24: Analysis of resilient modulus test 1 for Elsinore material.

Table D-26: Results of Resilient Modulus Test 2 for Elsinore Material

Sequence	Stress Invariant (psi)	Resilient Modulus (ksi)
1	11.6993	9.0
2	14.4014	6.3
3	17.0822	5.2
4	19.4934	12.4
5	24.0038	8.8
6	28.4943	7.0
7	38.9675	19.0
8	47.9596	13.2
9	56.9358	10.7
10	53.9566	30.1
11	58.4614	23.6
12	71.9782	17.4
13	73.4747	34.3
14	77.9671	29.9
15	95.9560	21.5

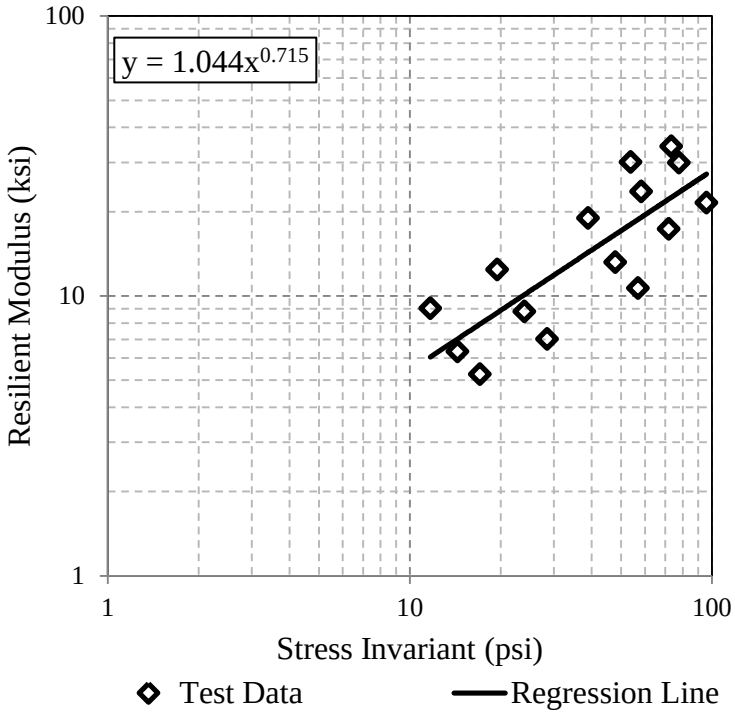

Figure D-25: Analysis of resilient modulus test 2 for Elsinore material.

Table D-27: Results of Resilient Modulus Test 3 for Elsinore Material

Sequence	Stress Invariant (psi)	Resilient Modulus (ksi)
1	11.7007	9.9
2	14.4027	6.3
3	17.0652	4.8
4	19.5018	11.3
5	23.9998	7.7
6	28.5106	6.2
7	38.9680	16.0
8	47.9497	11.6
9	56.9497	9.5
10	53.9624	26.0
11	58.4680	19.5
12	71.9470	15.1
13	73.4863	28.2
14	78.0006	24.7
15	95.9394	18.9

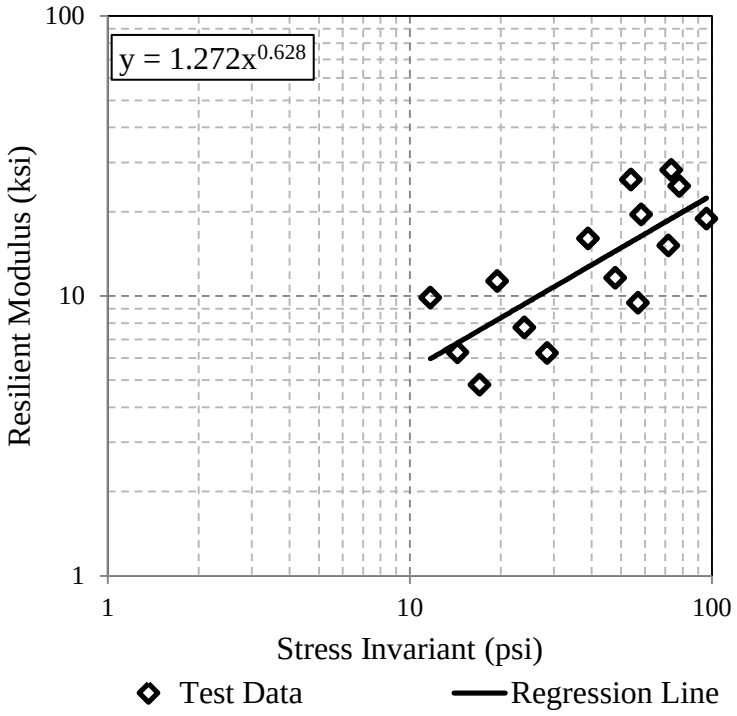

Figure D-26: Analysis of resilient modulus test 3 for Elsinore material.

Table D-28: Results of Resilient Modulus Test 4 for Elsinore Material

Sequence	Stress Invariant (psi)	Resilient Modulus (ksi)
1	11.6903	12.6
2	14.3971	7.2
3	17.1090	5.4
4	19.5069	15.8
5	23.9829	9.4
6	28.5101	7.0
7	38.9614	25.4
8	47.9362	14.8
9	56.9524	10.6
10	53.9747	45.5
11	58.4930	32.0
12	71.9426	18.8
13	73.4714	49.6
14	77.9718	39.5
15	95.9786	22.8

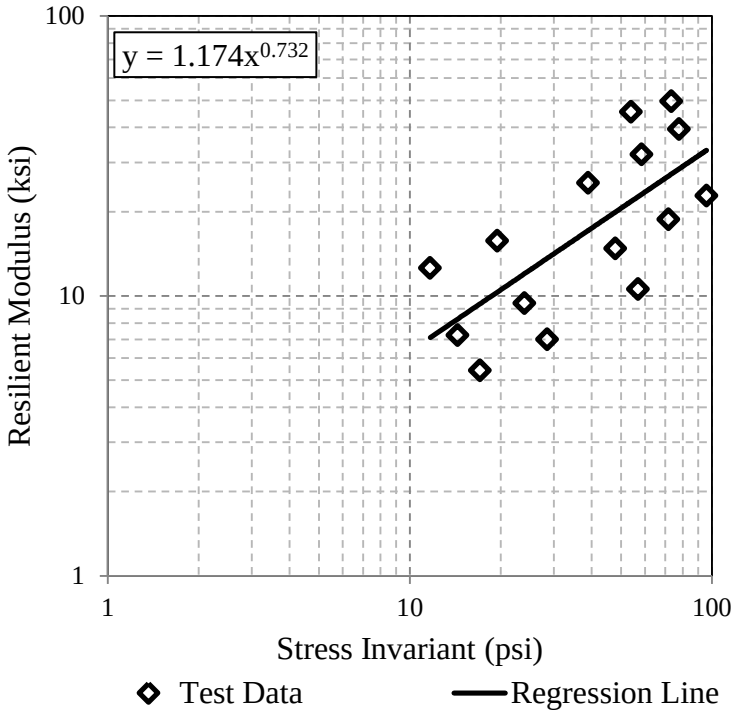

Figure D-27: Analysis of resilient modulus test 4 for Elsinore material.

Table D-29: Results of Resilient Modulus Test 1 for Nielson Material

Sequence	Stress Invariant (psi)	Resilient Modulus (ksi)
1	11.7012	23.6
2	14.3889	13.0
3	17.0843	9.7
4	19.5114	29.9
5	23.9933	17.4
6	28.4905	12.3
7	38.9489	44.4
8	47.9677	24.5
9	56.9515	16.6
10	53.9451	74.6
11	58.4762	51.9
12	71.9471	29.1
13	73.4814	79.4
14	77.9701	62.2
15	95.9717	34.1

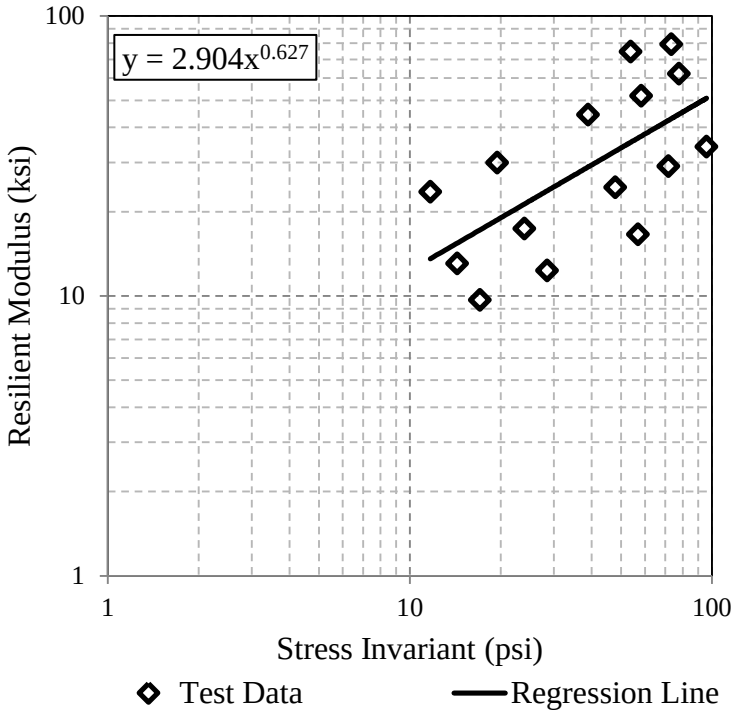

Figure D-28: Analysis of resilient modulus test 1 for Nielson material.

Table D-30: Results of Resilient Modulus Test 2 for Nielson Material

Sequence	Stress Invariant (psi)	Resilient Modulus (ksi)
1	11.6858	11.6
2	14.4045	7.6
3	17.1056	5.9
4	19.4925	13.3
5	24.0068	9.6
6	28.5132	7.5
7	38.9561	20.9
8	47.9558	13.9
9	56.9506	11.0
10	53.9662	32.0
11	58.4531	25.3
12	71.9846	17.9
13	73.5012	37.0
14	77.9755	32.4
15	95.9611	21.8

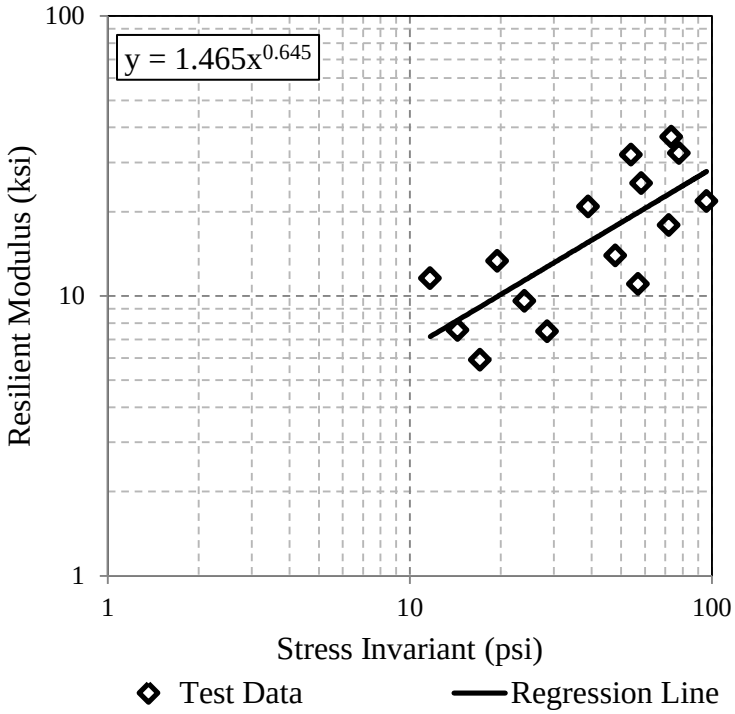

Figure D-29: Analysis of resilient modulus test 2 for Nielson material.

Table D-31: Results of Resilient Modulus Test 3 for Nielson Material

Sequence	Stress Invariant (psi)	Resilient Modulus (ksi)
1	11.6941	12.0
2	14.4012	8.1
3	17.0958	6.4
4	19.4904	14.8
5	23.9863	10.6
6	28.5053	8.1
7	38.9501	21.7
8	47.9647	14.7
9	56.9470	11.4
10	53.9726	31.9
11	58.4774	25.6
12	71.9646	18.5
13	73.4777	36.9
14	77.9790	32.5
15	95.9730	22.2

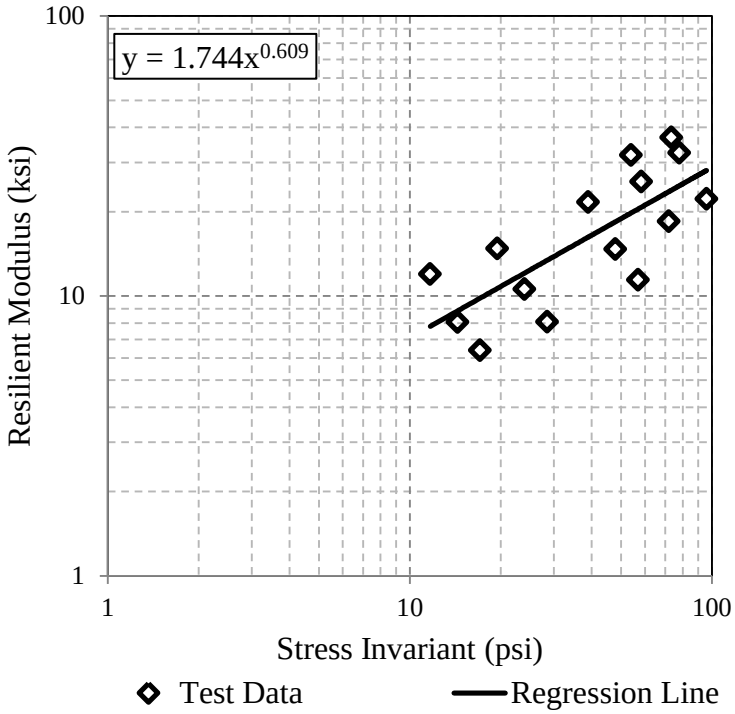

Figure D-30: Analysis of resilient modulus test 3 for Nielson material.

Table D-32: Results of Resilient Modulus Test 4 for Nielson Material

Sequence	Stress Invariant (psi)	Resilient Modulus (ksi)
1	11.6829	21.5
2	14.4047	12.1
3	17.0811	9.2
4	19.5085	26.6
5	23.9884	16.0
6	28.5002	11.5
7	38.9545	38.9
8	47.9539	22.6
9	56.9352	15.7
10	53.9519	62.4
11	58.4657	46.0
12	71.9550	27.3
13	73.4716	69.4
14	77.9673	56.2
15	95.9406	32.5

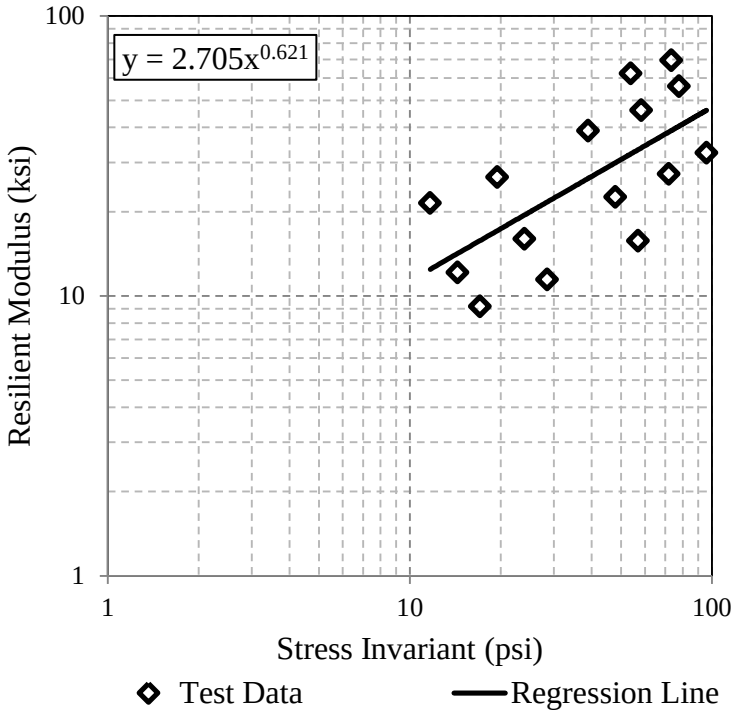

Figure D-31: Analysis of resilient modulus test 4 for Nielson material.

APPENDIX E RESULTS OF STATISTICAL ANALYSIS

Best Subsets Regression: Mr/RD versus P200, D30, OMC, MDD

Response is Mr/RD

Vars	R-Sq	R-Sq(adj)	Mallows Cp	S	P200	D30	OMC	MDD
1	42.8	31.3	29.2	2.0123				X
1	36.8	24.1	32.6	2.1145			X	
2	65.5	48.3	18.4	1.7458			X	X
2	58.2	37.3	22.5	1.9223	X			X
3	93.0	86.0	4.9	0.90762	X	X		X
3	71.2	42.4	17.2	1.8424		X	X	X
4	96.4	89.3	5.0	0.79266	X	X	X	X

INCLUDING ALL MATERIALS

Regression Analysis: Mr/RD versus P200, D30, OMC, MDD

The regression equation is
Mr/RD = - 200 - 1.51 P200 - 418 D30 - 3.09 OMC + 1.94 MDD

Predictor	Coef	SE Coef	T	P
Constant	-199.96	54.28	-3.68	0.035
P200	-1.5111	0.3893	-3.88	0.030
D30	-418.42	85.24	-4.91	0.016
OMC	-3.091	1.169	-2.64	0.077
MDD	1.9412	0.3987	4.87	0.017

S = 0.792197 R-Sq = 96.8% R-Sq(adj) = 92.6%

Analysis of Variance

Source	DF	SS	MS	F	P
Regression	4	57.552	14.388	22.93	0.014
Residual Error	3	1.883	0.628		
Total	7	59.434			

Source	DF	Seq SS
P200	1	0.697
D30	1	0.240
OMC	1	41.741
MDD	1	14.874

EXCLUDING MCGUIRE

Regression Analysis: Mr/RD versus P200, D30, OMC, MDD

The regression equation is
Mr/RD = - 200 - 1.51 P200 - 418 D30 - 3.09 OMC + 1.94 MDD

Predictor	Coef	SE Coef	T	P
Constant	-199.82	70.25	-2.84	0.105
P200	-1.5103	0.4940	-3.06	0.092
D30	-418.2	112.1	-3.73	0.065
OMC	-3.094	1.485	-2.08	0.173
MDD	1.9401	0.5157	3.76	0.064

S = 0.970230 R-Sq = 96.8% R-Sq(adj) = 90.5%

Analysis of Variance

Source	DF	SS	MS	F	P
Regression	4	57.356	14.339	15.23	0.063
Residual Error	2	1.883	0.941		
Total	6	59.239			

Source	DF	Seq SS
P200	1	1.086
D30	1	0.428
OMC	1	42.519
MDD	1	13.323

EXCLUDING TRENTON

Regression Analysis: Mr/RD versus P200, D30, OMC, MDD

The regression equation is
Mr/RD = - 258 - 1.92 P200 - 469 D30 - 2.62 OMC + 2.38 MDD

Predictor	Coef	SE Coef	T	P
Constant	-258.05	48.56	-5.31	0.034
P200	-1.9187	0.3456	-5.55	0.031
D30	-469.02	65.91	-7.12	0.019
OMC	-2.6195	0.8667	-3.02	0.094
MDD	2.3771	0.3596	6.61	0.022

S = 0.564454 R-Sq = 98.7% R-Sq(adj) = 96.2%

Analysis of Variance

Source	DF	SS	MS	F	P
Regression	4	49.781	12.445	39.06	0.025
Residual Error	2	0.637	0.319		
Total	6	50.419			

Source	DF	Seq SS
P200	1	0.066
D30	1	1.300
OMC	1	34.495
MDD	1	13.921

EXCLUDING BECK ST.

Regression Analysis: Mr/RD versus P200, D30, OMC, MDD

The regression equation is
Mr/RD = - 197 - 1.64 P200 - 467 D30 - 3.31 OMC + 1.96 MDD

Predictor	Coef	SE Coef	T	P
Constant	-197.36	50.74	-3.89	0.060
P200	-1.6424	0.3797	-4.33	0.050
D30	-466.76	89.24	-5.23	0.035
OMC	-3.312	1.108	-2.99	0.096
MDD	1.9555	0.3726	5.25	0.034

S = 0.739962 R-Sq = 98.1% R-Sq(adj) = 94.4%

Analysis of Variance

Source	DF	SS	MS	F	P
Regression	4	58.009	14.502	26.49	0.037
Residual Error	2	1.095	0.548		
Total	6	59.104			

Source	DF	Seq SS
P200	1	0.426
D30	1	0.968
OMC	1	41.537
MDD	1	15.078

Unusual Observations

Obs	P200	Mr/RD	Fit	SE Fit	Residual	St Resid
5	5.4	25.403	25.447	0.737	-0.044	-0.66 X

X denotes an observation whose X value gives it large leverage.

EXCLUDING PARLEY'S CANYON

Regression Analysis: Mr/RD versus P200, D30, OMC, MDD

The regression equation is
Mr/RD = - 189 - 1.40 P200 - 410 D30 - 3.46 OMC + 1.87 MDD

Predictor	Coef	SE Coef	T	P
Constant	-189.12	73.46	-2.57	0.124
P200	-1.3975	0.5888	-2.37	0.141
D30	-409.8	105.5	-3.88	0.060
OMC	-3.463	1.829	-1.89	0.199
MDD	1.8711	0.5261	3.56	0.071

S = 0.947030 R-Sq = 96.9% R-Sq(adj) = 90.8%

Analysis of Variance

Source	DF	SS	MS	F	P
Regression	4	56.993	14.248	15.89	0.060
Residual Error	2	1.794	0.897		
Total	6	58.787			

Source	DF	Seq SS
P200	1	3.355
D30	1	0.652
OMC	1	41.643
MDD	1	11.344

EXCLUDING POINT OF THE MOUNTAIN

Regression Analysis: Mr/RD versus P200, D30, OMC, MDD

The regression equation is
Mr/RD = - 148 - 1.20 P200 - 349 D30 - 3.28 OMC + 1.54 MDD

Predictor	Coef	SE Coef	T	P
Constant	-147.78	50.84	-2.91	0.101
P200	-1.1979	0.3459	-3.46	0.074
D30	-349.22	75.91	-4.60	0.044
OMC	-3.2807	0.8994	-3.65	0.068
MDD	1.5367	0.3805	4.04	0.056

S = 0.605042 R-Sq = 97.6% R-Sq(adj) = 92.9%

Analysis of Variance

Source	DF	SS	MS	F	P
Regression	4	30.0217	7.5054	20.50	0.047
Residual Error	2	0.7322	0.3661		
Total	6	30.7539			

Source	DF	Seq SS
P200	1	1.4588
D30	1	0.5931
OMC	1	21.9993
MDD	1	5.9705

EXCLUDING VERNAL

Regression Analysis: Mr/RD versus P200, D30, OMC, MDD

The regression equation is
Mr/RD = - 243 - 1.81 P200 - 493 D30 - 2.15 OMC + 2.25 MDD

Predictor	Coef	SE Coef	T	P
Constant	-242.7	143.5	-1.69	0.233
P200	-1.812	1.015	-1.78	0.216
D30	-493.4	246.9	-2.00	0.184
OMC	-2.151	3.146	-0.68	0.565
MDD	2.249	1.039	2.16	0.163

S = 0.944355 R-Sq = 97.0% R-Sq(adj) = 91.0%

Analysis of Variance

Source	DF	SS	MS	F	P
Regression	4	57.639	14.410	16.16	0.059
Residual Error	2	1.784	0.892		
Total	6	59.422			

Source	DF	Seq SS
P200	1	0.704
D30	1	0.404
OMC	1	52.353
MDD	1	4.177

EXCLUDING ELSINORE

Regression Analysis: Mr/RD versus P200, D30, OMC, MDD

The regression equation is
Mr/RD = - 203 - 1.47 P200 - 425 D30 - 3.57 OMC + 1.98 MDD

Predictor	Coef	SE Coef	T	P
Constant	-202.77	48.94	-4.14	0.054
P200	-1.4663	0.3523	-4.16	0.053
D30	-424.53	76.93	-5.52	0.031
OMC	-3.574	1.116	-3.20	0.085
MDD	1.9807	0.3605	5.49	0.032

S = 0.713606 R-Sq = 98.1% R-Sq(adj) = 94.4%

Analysis of Variance

Source	DF	SS	MS	F	P
Regression	4	53.439	13.360	26.24	0.037
Residual Error	2	1.018	0.509		
Total	6	54.458			

Source	DF	Seq SS
P200	1	2.806
D30	1	0.014
OMC	1	35.245
MDD	1	15.375

EXCLUDING NIELSON

Regression Analysis: Mr/RD versus P200, D30, OMC, MDD

The regression equation is
Mr/RD = - 206 - 1.47 P200 - 384 D30 - 2.12 OMC + 1.93 MDD

Predictor	Coef	SE Coef	T	P
Constant	-206.13	54.66	-3.77	0.064
P200	-1.4746	0.3912	-3.77	0.064
D30	-383.63	92.13	-4.16	0.053
OMC	-2.118	1.523	-1.39	0.299
MDD	1.9271	0.3992	4.83	0.040

S = 0.792658 R-Sq = 96.4% R-Sq(adj) = 89.3%

Analysis of Variance

Source	DF	SS	MS	F	P
Regression	4	34.1104	8.5276	13.57	0.070
Residual Error	2	1.2566	0.6283		
Total	6	35.3670			

Source	DF	Seq SS
P200	1	0.3491
D30	1	6.9563
OMC	1	12.1649
MDD	1	14.6401

Unusual Observations

Obs	P200	Mr/RD	Fit	SE Fit	Residual	St Resid
3	11.3	20.276	20.216	0.789	0.060	0.79 X

X denotes an observation whose X value gives it large leverage.